

University of Windsor

Scholarship at UWindor

Electronic Theses and Dissertations

Theses, Dissertations, and Major Papers

2-16-2016

Commissioning and Performance Analysis of WhisperGen Stirling Engine

Prashant Kaliram Pradip
University of Windsor

Follow this and additional works at: <https://scholar.uwindsor.ca/etd>

Recommended Citation

Pradip, Prashant Kaliram, "Commissioning and Performance Analysis of WhisperGen Stirling Engine" (2016). *Electronic Theses and Dissertations*. 5661.
<https://scholar.uwindsor.ca/etd/5661>

This online database contains the full-text of PhD dissertations and Masters' theses of University of Windsor students from 1954 forward. These documents are made available for personal study and research purposes only, in accordance with the Canadian Copyright Act and the Creative Commons license—CC BY-NC-ND (Attribution, Non-Commercial, No Derivative Works). Under this license, works must always be attributed to the copyright holder (original author), cannot be used for any commercial purposes, and may not be altered. Any other use would require the permission of the copyright holder. Students may inquire about withdrawing their dissertation and/or thesis from this database. For additional inquiries, please contact the repository administrator via email (scholarship@uwindsor.ca) or by telephone at 519-253-3000ext. 3208.

Commissioning and Performance Analysis of WhisperGen Stirling Engine

By

Prashant Kaliram Pradip

A Thesis

Submitted to the Faculty of Graduate Studies
through the Department of Mechanical, Automotive and Materials Engineering
in Partial Fulfillment of the Requirements for
the Degree of Master of Applied Science
at the University of Windsor

Windsor, Ontario, Canada

2016

© 2016 Prashant Kaliram Pradip

Commissioning and Performance Analysis of WhisperGen Stirling Engine

By

Prashant Kaliram Pradip

APPROVED BY:

Dr. Paul Henshaw, Outside Reader

Department of Civil and Environmental Engineering

Dr. Ming Zheng, Program Reader

Department of Mechanical, Automotive and Materials Engineering

Dr. David S-K Ting, Advisor

Department of Mechanical, Automotive and Materials Engineering

Dr. Graham T Reader, Advisor

Department of Mechanical, Automotive and Materials Engineering

February 4,2016

DECLARATION OF ORIGINALITY

I hereby certify that I am the sole author of this thesis and that no part of this thesis has been published or submitted for publication.

I certify that, to the best of my knowledge, my thesis does not infringe upon anyone's copyright nor violate any proprietary rights and that any ideas, techniques, quotations, or any other material from the work of other people included in my thesis, published or otherwise, are fully acknowledged in accordance with the standard referencing practices. Furthermore, to the extent that I have included copyrighted material that surpasses the bounds of fair dealing within the meaning of the Canada Copyright Act, I certify that I have obtained a written permission from the copyright owner(s) to include such material(s) in my thesis and have included copies of such copyright clearances to my appendix.

I declare that this is a true copy of my thesis, including any final revisions, as approved by my thesis committee and the Graduate Studies office, and that this thesis has not been submitted for a higher degree to any other University or Institution.

ABSTRACT

Stirling engine based cogeneration systems have potential to reduce energy consumption and greenhouse gas emission, due to their high cogeneration efficiency and emission control due to steady external combustion. To date, most studies on this unit have focused on performance based on both experimentation and computer models, and lack experimental data for diversified operating ranges.

This thesis starts with the commissioning of a WhisperGen Stirling engine with components and instrumentation to evaluate power and thermal performance of the system. Next, a parametric study on primary engine variables, including air, diesel, and coolant flowrate and temperature were carried out to further understand their effect on engine power and efficiency. Then, this trend was validated with the thermodynamic model developed for the energy analysis of a Stirling cycle. Finally, the energy balance of the Stirling engine was compared without and with heat recovery from the engine block and the combustion chamber exhaust.

DEDICATION

This work is dedicated to my father Pradip Ganesan and my mother Pushpavalli Pradip.

ACKNOWLEDGEMENTS

I would like to express my sincere gratitude to my supervisors Dr. David S-K Ting and Dr. Graham T Reader without whom I would not have got the opportunity to join this wonderful research group. Their excellent guidance and support during my MASc Program have been a consistent encouragement for this thesis work. I would also like to thank them for all the other help they have provided in my academic life and beyond.

I am deeply grateful to the invaluable comments from the committee members Dr. Ming Zheng and Dr. Paul Henshaw. Also, would like to thank University of Toronto Professor Murray J. Thomson for lending WhisperGen MicroCHP.

My sincere thanks to Mr. Bruce Durfy, Mr. Dean Poublon, Mr. Andy Jenner, Mr. Patrick Seguin, and Mr. Frank Cicchello who gave me valuable technical assistance on the fabrication of various hardware components used in this research. Much appreciation is extended to Mr. Jan Barmantloo of Off-Grid Energy, in New Zealand, for particularly with understanding the engine's inner workings and debugging control system issues.

I wish to extend my acknowledgement to everyone in the Turbulence and Energy Laboratory at the University of Windsor. Thankful for the financial support from the Clean Diesel Engine Laboratory, Department of Mechanical, Automotive and Materials Engineering in the form of Graduate Assistantships, Natural Sciences and Engineering Research Council of Canada.

Last but not least, my immense appreciation, and sincere thanks to my parents and my friend Vimal and family for their unconditional support, constant love, and encouragement during my study.

TABLE OF CONTENTS

DECLARATION OF ORIGINALITY	iii
ABSTRACT	iv
DEDICATION	v
ACKNOWLEDGEMENTS	vi
LIST OF TABLES	x
LIST OF FIGURES	xi
LIST OF ABBREVIATIONS / SYMBOLS	xiv
CHAPTER 1 INTRODUCTION AND LITERATURE REVIEW	1
1.1 Motivation	1
1.2 Background	1
1.2.1 Ideal Stirling Cycle	2
1.2.2 Non Idealized Behavior	3
1.2.3 Engine Configuration	5
1.2.4 Commercial Engine and Applications	6
1.3 WhisperGen MicroCHP	8
1.4 Literature Review	11
1.5 Objectives	12
1.6 Outline of Thesis	12
CHAPTER 2 THERMODYNAMIC ANALYSIS	14
2.1 Energy Balance of a Stirling Engine	14
2.1.1 Power Efficiency	15
2.1.2 Energy Losses	15
2.1.3 Preheating	16
2.2 Energy Balance with Heat Recovery	16

2.3 Stirling Cycle Analysis	17
2.3.1 Dead Volumes	18
2.3.2 Regenerator Effectiveness and Temperature	20
2.3.3 Irreversibility Parameter	21
2.3.4 Conductive Loss	21
2.3.5 Cyclic Processes	21
2.3.6 Total Heat Added	23
2.3.7 Total Heat Rejected	23
2.3.8 Cyclic Power and Efficiency	24
2.4 Non Dimensional Analysis	24
2.4.1 Beale formula	24
2.4.2 West formula	25
CHAPTER 3 EXPERIMENTAL METHODOLOGY	26
3.1 Experimental Installation	26
3.1.1 Air Supply System	26
3.1.2 Fuel Supply System	28
3.1.3 Burner Assembly	28
3.1.4 Exhaust System	30
3.1.5 Cooling System	30
3.1.6 Electrical System	31
3.2 Data Acquisition System	32
3.2.1 Sensors	32
3.2.1.1 Temperature Sensor	32
3.2.1.2 Flame Ionization Detector	33
3.2.1.3 Oxygen Sensor	33
3.2.1.4 Flowmeter	34
3.2.1.5 Voltmeter and Ammeter	34
3.2.2 Sensor Calibration	34
3.2.3 Uncertainty Analysis	35
3.2.4 Data Logging Software	36
3.2.4.1 Micromon	36

3.2.4.2 LabVIEW	37
3.3 Operating Procedure	37
CHAPTER 4 RESULTS AND DISCUSSION	40
4.1 Engine Operation	40
4.2 Engine Performance	45
4.3 Reproducibility and Uncertainty	46
4.4 Parametric Study	47
4.4.1 Inlet Air Temperature	48
4.4.2 Air Flowrate	48
4.4.3 Diesel Flowrate	50
4.4.4 Coolant Flowrate	51
4.4.5 Coolant Inlet Temperature	52
4.4.6 Coolant Outlet Temperature	53
4.5 Beale Number Analysis	55
4.6 Engine Performance with Heat Recovery	55
4.6.1 Parametric Study of Water Flowrate	58
CHAPTER 5 CONCLUSIONS AND RECOMMENDATIONS	60
5.1 Conclusions	60
5.2 Recommendations	61
REFERENCES	63
VITA AUCTORIS	69

LIST OF TABLES

Table 1-1 Properties of common Stirling engine working fluids	5
Table 1-2 Manufacturers of Stirling engine systems	7
Table 1-3 Specifications of WhisperGen MicroCHP	9
Table 2-1 Constants used in Stirling cycle analysis	20
Table 3-1 Temperatures measured and instrumentation	33
Table 4-1 Engine parameters and performance for multiple tests	47
Table 4-2 Test parameters	47

LIST OF FIGURES

Figure 1-1 P - V and T - S plots of ideal Stirling cycle	2
Figure 1-2 Stirling engine piston cylinder configurations	5
Figure 1-3 Four-cylinder double acting configuration	6
Figure 1-4 Diesel fueled WhisperGen MicroCHP	8
Figure 1-5 WhisperGen MicroCHP control / data transfer	10
Figure 2-1 Thermodynamic model of Stirling engine system	15
Figure 2-2 Thermodynamic model of preheating ambient air	16
Figure 2-3 Thermodynamic model of Stirling engine with heat recovery	17
Figure 2-4 P - V and T - S diagrams for Stirling cycle	18
Figure 2-5 State diagram with volumes of Stirling cycle	19
Figure 2-6 Beale number as function of source temperature	25
Figure 3-1 Layout of WhisperGen experimental setup	27
Figure 3-2 Photograph of WhisperGen test setup	27
Figure 3-3 Layout of fuel delivery system	28
Figure 3-4 Schematic of burner assembly	29
Figure 3-5 Photograph of internal heat exchanger	29
Figure 3-6 Layout of cooling system	31

Figure 3-7 Schematic of electrical system	32
Figure 3-8 Screenshot of WhisperGen control software Micromon	36
Figure 3-9 Engine test procedure flow diagram	37
Figure 4-1 Air flowrate	41
Figure 4-2 Diesel consumption	42
Figure 4-3 Fuel air equivalence ratio	42
Figure 4-4 Oxygen concentration	43
Figure 4-5 System temperatures variation	44
Figure 4-6 Electrical output	45
Figure 4-7 Electrical efficiency	46
Figure 4-8 Inlet air temperature study	49
Figure 4-9 Air flowrate study	50
Figure 4-10 Diesel flowrate study	51
Figure 4-11 Coolant flowrate study	52
Figure 4-12 Coolant inlet temperature study	53
Figure 4-13 Coolant outlet temperature study	54
Figure 4-14 Quantitative estimate of Beale number	55
Figure 4-15 Energy balance of WhisperGen with heat recovery	56
Figure 4-16 Energy balance without heat recovery	57
Figure4-17 LHV efficiencies of WhisperGen system	58

LIST OF ABBREVIATIONS / SYMBOLS

B	Bias
B_N	Beale Number
c_p	Specific Heat at Constant Pressure (kJ/kg·K)
D	Dead Volume Parameter
F	Flowmeter (l/min)
h	Specific Enthalpy (kJ/kg)
k	Specific Heat Ratio
LHV	Lower Heating Value (kJ/kg·K)
m	Mass (kg)
\dot{m}	Mass Flowrate (kg/s)
N	Engine Speed (RPM)
P	Pressure (Pa)
\dot{Q}	Thermal Power (W)
R	Gas Constant (kJ/kg·K)
S	precision index
T	Temperature (K)
t	Student's t Value
U	Uncertainty
V	Volume (m ³)
\dot{W}	Work (J)
W_N	West Number
x/y	Data

Greek

ε	Effectiveness
---------------	---------------

η	Efficiency (%)
\emptyset	Equivalence Ratio
f	Cycle Frequency (Hz)

Subscripts

1 1' 2 3 3' 4	States
A	Air
avg	Average
B	Burner
C	Coolant / Cold Space / Compression Space
D	Diesel Fuel
DC	Dead Volume at Compression Space
DE	Dead Volume at Expansion Space
DR	Volume at Regenerator
DT	Total Dead Volume
E	Exhaust
El	Electrical
H	Hot Space / Expansion Space
i	interval
L	Loss
O	Ambient
R	Regenerator
S	Swept Volume
T	Total
Th	Thermal
W	Water

CHAPTER 1

INTRODUCTION AND LITERATURE REVIEW

1.1 Motivation

Increase in fuel prices, depletion of fossil fuels, negative environmental impact, and issues of providing remote communities with electricity have brought major involvement of governments of Canada and others around the world to develop energy generation locally. According to the Energy Information Administration [1] Canada's carbon dioxide emissions increased by 1% per year from 2009 to 2020, so immediate action is required to reduce greenhouse gas emissions in all energy consuming sectors.

One particular technology for efficient use of energy and reduced effect on environment is cogeneration. Cogeneration is simultaneous production of more than one useful form of energy (such as electrical power and heat) and this currently represents only 7% of electricity produced in Canada [1]. This mode of operation always results in better utilization of a single form of input energy and offers high economic benefits and low greenhouse gas emissions. Furthermore, combined heat and power systems based on the Stirling engine have a very high efficiency and wide variety of applications, ranging from the residential sector (< 10 kW), and waste heat recovery. In the Northern part of Canada, diesel generators are very common, so Stirling engine MicroCHP's with state-of-the-art diesel burners would produce less climatic impact, as power can be generated on site in addition to capturing the waste heat from combustion.

1.2 Background

The hot air regenerative engine (Stirling engine) is a reciprocating external combustion engine which operates on a closed thermodynamic cycle and was invented, and patented by Robert Stirling in 1816 [2]. There are many benefits associated with

Stirling engine, including high efficiency, flexibility of fuels, quiet operation, and long, maintenance-free run time [3]. Unlike the internal combustion engine, heat energy is produced externally in the Stirling engine. As a result, a wide range of heat sources can be used, including conventional fossil fuels, renewable energy sources such as biomass and solar energy, and recovered waste heat. Also, due to steady external combustion, the combustion process can be well controlled resulting in less emissions than an internal combustion engine with a catalytic converter. Finally, in spite of being expensive for production, their benefits exceed the cost in combined heat and power, or cogeneration [4].

1.2.1 Ideal Stirling Cycle

A Stirling engine operates on a closed regenerative cycle known as the Stirling cycle, where a working fluid is contained within the thermodynamic system and completely independent of the combustion process. The cycle operates on four processes, which are outlined in the pressure-volume and temperature-enthalpy plots in Figure 1-1. In process 1-2 heat is added to the system from the heat source. The working fluid undergoes isothermal expansion; the volume increases and pressure decreases as the working fluid expands at constant temperature. Process 2-3 is isochoric cooling; the pressure decreases at constant volume as the gas is cooled. No work is being done either on the system or by the system and all thermal energy is absorbed by the regenerator, causing a decrease in

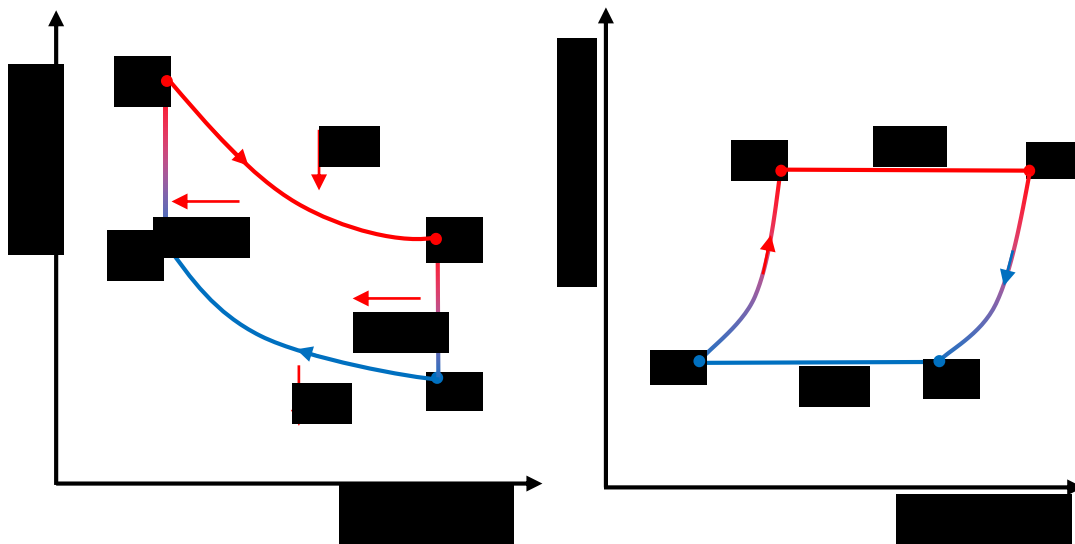


Figure 1-1 P - V and T - S plots of ideal Stirling cycle

internal energy of the working fluid. Process 3-4 is isothermal compression; the volume decreases and pressure increases as the working fluid is compressed at constant temperature. The heat is rejected to the engine coolant or heat sink. Process 4-1 is isochoric heating; the pressure increases at constant volume as the gas is heated up by the regenerator. No work is being done either on the system or by the system and all thermal energy gained causes an increase in internal energy [5].

1.2.2 Non Idealized Behavior

The ideal Stirling cycle efficiency is equal to the Carnot efficiency, but an actual Stirling engine has many deficiencies, such as dead volumes, imperfect regenerators, heat losses, etc. that limit the maximum practical efficiency. Further, the complex drive mechanism and components (heater, regenerator, and cooler) implemented in the Stirling engine leads to losses due to friction, working fluid leakages, heat losses and mechanical losses [6].

Material: Operation of a Stirling engine relies primarily on the heat transfer between the working fluid and the heat source, and sink. So a material must be chosen with high level of thermal conductivity, preferable copper (398 W/m·K) or aluminum (237 W/m·K) [7] for better heat transfer.

Heat Transfer: Stirling engines have variable volume cylinders that do not provide sufficient heat transfer, resulting in little heat being transferred to the working fluid. The hot and cold cylinders lead to convectional losses. These make the whole process deviate from the ideal isothermal mode, and can result in a 40% reduction in power efficiency [8].

Working Pressure: The working fluid interacting with the piston cylinder walls introduces friction and gas flow inside the regenerator causing flow friction, resulting in pressure drop. Another issue is the leakage of working fluid through seals and connections due to high pressurization. This pressure loss can account for up to 10% loss of power efficiency [9].

Mechanical Loss: These losses are incurred from the drive shaft, bearings and other engine components which transfer the linear piston motion for power production. An optimal mechanism for the Stirling engine should be simple and reliable, so it will generate only

small slide-forces. Slide-forces not only threaten sealing surfaces, they also directly increase friction and thus reduce mechanical efficiency of the engine [10].

Dead Volume: Working fluid contained in the hot and cold side heat exchangers, regenerator, piston cylinder clearances, and connecting ducts are dead volumes. This is not included in the swept volume of the piston and this fluid affects the power output of the engine. In a typical Stirling engine, about 50% of the total volume is dead volume and this linearly decreases the engine's power output [11].

Regenerator: One of the most important parts of the Stirling engine is the regenerator, which is a thermal storage device and is typically made from stainless steel or ceramic mesh. The function of a regenerator is to absorb heat when hot gas passes from the hot side to cold side and to release that heat internally when cold gas pass through it, to improve the efficiency of the process. Next, being positioned between the hot and cold side heat exchangers, the regenerator can also reduce conductive losses. But, this regeneration cannot be perfect and the imperfect regenerator accounts for up to 20% decrease from Carnot efficiency [12].

Working Fluid: A major factor affecting performance of a Stirling engine is the choice of working fluid. To maximize performance, the working fluid should have a high thermal conductivity. To provide increased heat transfer rate, it should have a low heat capacity so there will be a large change in temperature for a small energy input. And it should have a low viscosity for reduced frictional losses. Some typical working fluids are listed in Table 1-1. Hydrogen is an excellent candidate, but safety issues, high flammability, and high diffusion rate in metals makes containment extremely hazardous [13]. The next best option is helium due to its inert nature, even though its viscosity is twice as that of hydrogen. However, nitrogen and air are typically used, due to their availability and safe for high pressure applications.

1.2.3 Engine Configuration

Stirling engines are classified by their piston cylinder arrangement and drive mechanism [14]. Figure 1-2 shows the three different mechanical configurations: alpha, beta and gamma. These configurations can be either single or double acting mode of

Table 1-1 Properties of common Stirling engine working fluids [7]

	Hydrogen	Helium	Nitrogen	Air
Thermal conductivity (W/m·K)	0.1805	0.1513	0.02583	0.0239
Specific heat (kJ/kg·K)	14.32	5.19	1.04	1.01
Viscosity (Pa·s)	0.0088	0.0190	0.0178	0.0183

operation. In the single acting mode, only one side of the piston is in contact with the working fluid. On the other hand, double acting engines have working fluid on both sides of the displacer, i.e. the expansion space of one cylinder is connected to the compression space of the same or another cylinder.

An alpha type engine has two pistons and cylinders, expansion and compression work takes place in separate cylinders and the main drawback is that both pistons have to be sealed in order to contain the working fluid. Beta type engines employ a displacer and a piston inside the cylinder. The displacer piston is used to move working fluid between the hot space, regenerator and cold space, and cannot be coupled to the engine's power piston. Alternatively, it can be connected to crankshaft through mechanical linkages. A

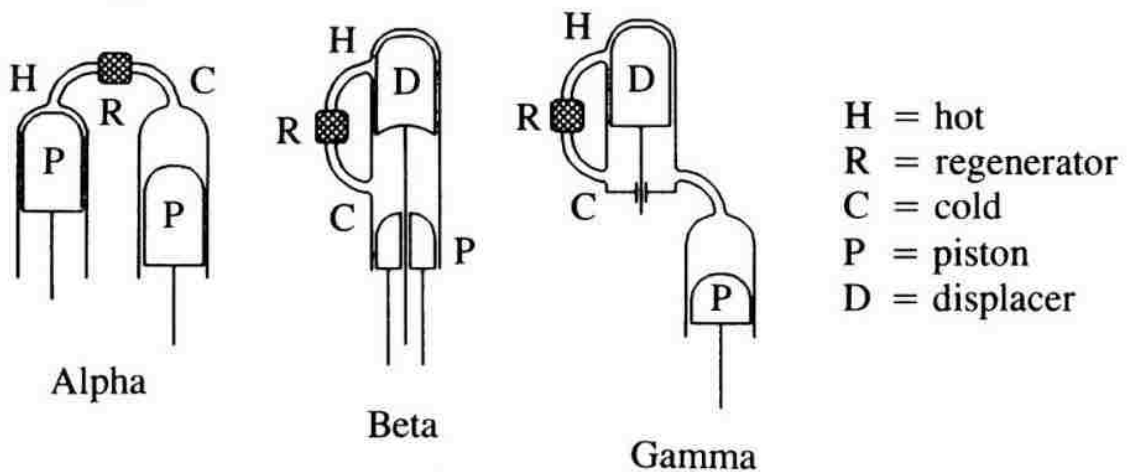


Figure 1-2 Stirling engine piston cylinder configurations [10]

gamma type engine also employs a displacer and a piston, but located in different cylinders, where the working fluid is passed from displacer cylinder through heater, regenerator, and cooler to a piston connected cylinder.

The four-cylinder double acting configuration is a variation of the alpha type engine, where cylinders are interconnected, i.e. the working fluid expansion space in one cylinder is connected to another cylinder compression space via a regenerator (Figure 1-3). This arrangement allows multiple cylinder application and has proven high mechanical efficiency [15].

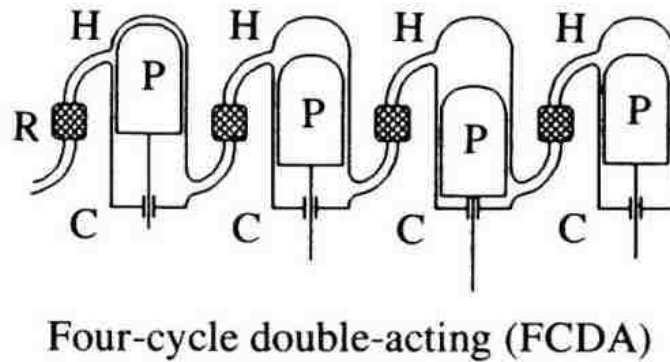


Figure 1-3 Four-cylinder double acting configuration [10]

The drive mechanism couples to engine's pistons for power production. Kinematic drive mechanical linkages are the most common ones, which include slider crank, rhombic drive, scotch yoke, wobble yoke, and swash plate. These mechanisms require special sealing to prevent leakages and to limit frictional losses. On the other hand, free piston technology was developed to overcome some of the mechanical linkage limitations; each piston is moved by working fluid pressure variation and the work is harnessed by an alternator [16].

1.2.4 Commercial Engines and Applications

A variety of companies have brought Stirling engine technology to the commercial stage, but today only a few companies are building and selling engines. Table 1-2 shows the recently developed systems along with their working fluid, fuel type, nominal power output and power efficiency. It should also be noted that most of these units are capable of operating with a range of fuels. In addition, these engines differ greatly when considering

the number of cylinders, mean pressures of the working fluid, and drive mechanism. This considerable variation in Stirling engine design results in wide range of systems with respect to scale and performance.

Table 1-2 Manufacturers of Stirling engine systems [15, 17]

Manufacturer	Working Fluid	Fuel	Power Output [kW]	Electrical Efficiency [%]
Cleanergy	Helium	Various	2 - 9	25
Cool Energy	Nitrogen	Various	25	30
Kockums	Hydrogen	Diesel	75	-
Mahle	Hydrogen	Natural gas	25	40.5
Microgen	Helium	Natural gas	1	-
Qnergy	Helium	Various	3 - 7.5	37
Ripasso	-	Solar	32	33
Solo	Helium	Natural gas	9	24
Stirling Power	Hydrogen	Various	43	-
Stirling Dk	Helium	Biomass	35 - 500	17
Sunpower	Helium	Various	7.5	40
Whispergen Tech	Nitrogen	Diesel / Natural gas	1	12

A Stirling engine was incorporated as a central component in many cogeneration systems. With biggest number of engines sold in the residential cogeneration market are mainly installed in European homes [18]. Further, solar Stirling engines were developed with greater focus on mass production and can be found in various test facilities [19]. Finally, Stirling engine technology developed by Kochums for submarines, is the most powerful engine in production today at 75 kW [20].

1.3 WhisperGen MicroCHP

Whisper Tech Limited is a New Zealand firm that has developed MicroCHP systems based on the Stirling engine for small scale applications. They have developed two product lines that include; an on-grid system fueled by natural gas, specially targeted for residential application and capable of exporting any unused electricity back to grid, and an off-grid system fueled by automotive grade diesel for marine and remote applications. A 12V DC WhisperGen MicroCHP burning diesel is utilized in this study, and schematic and specifications are illustrated in Figure 1-4 and Table 1-3, respectively. The system consists of a burner, Stirling engine, alternator and electrical controller in compact assembly. The burner has a continuous premixed combustor with a single swirl evaporator that provides approximately 750 K heat to the engine. Exhaust from the combustion chamber passes

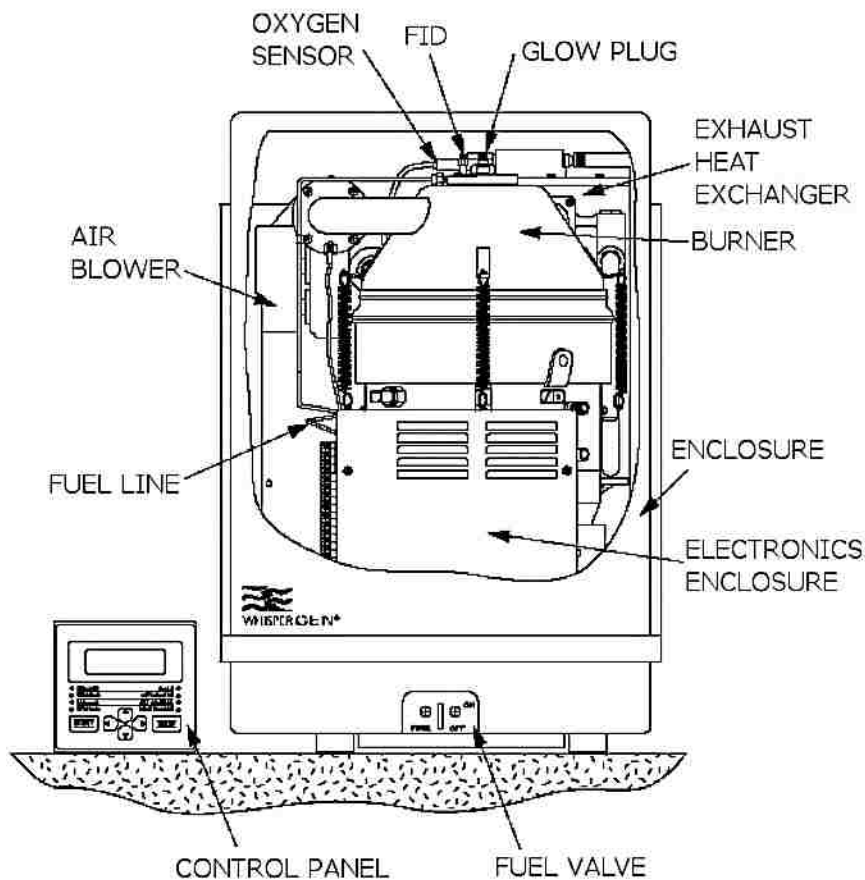


Figure 1-4 Diesel fueled WhisperGen MicroCHP [21]

through a plate heat exchanger which dumps heat from the exhaust in the same coolant which extracts heat from engine block. Cold start ignition of the engine is achieved by a glow plug and the refractory ceramic shell is used to provide high radiant heat transfer, and insulation.

Table 1-3 Specifications of WhisperGen MicroCHP [21]

Feature	Specification
Prime mover	4-cylinder alpha double acting Stirling cycle engine
Engine mechanism	Kinematic wobble yoke
Burner	Single nozzle swirl stabilized recuperating
Fuel	No. 2 diesel
Consumption	Max. 1 l/hr
Working fluid	Nitrogen
Hot nitrogen pressure	2.8 MPa
Coolant	glycol based antifreeze
Exhaust temperature	Max. 350 K
Parasitic load	75 W
Power output	1 kW nominal
Power efficiency	12%
Thermal output	8 kW nominal
Thermal efficiency	80%
Generator efficiency	90% (assumed)
Nominal voltage	12 V DC
Engine speed	1200 - 1500 RPM
Dry weight	120 kg
Dimensions	390 mm (width) x 550 mm (depth) x 850 mm (height)

The Stirling engine pistons are made of alloy steel and are sealed using PTFE lip seals backed with O-rings. The hot side heat exchangers are made of high temperature stainless steel for corrosion resistance; the cold side heat exchangers and regenerator are made of copper for a high heat transfer rate. The volumetric displacement of the engine is

101 cm³ (4 cm bore and 2 cm stroke) [22]. Mechanical motion of engine is created by continuous expansion and compression of the working fluid and charge pressure. A wobble yoke mechanism is used to convert linear motion to rotational motion with very low piston side loads.

AC electricity is produced by an alternator, which is converted to DC through series of rectifier and is stored in 12 V DC deep cycle lead acid battery. An inverter is used to convert 12 V DC to 120 V of AC power in order to power auxiliary devices. Then a shell and tube heat exchanger is used to extract thermal output, from coolant circulating in the engine block and also an exhaust heat exchanger by running laboratory cold water through the shell. The engine has various sensors for optimum operation, like an exhaust oxygen sensor, responsible for maintaining a fixed fuel-air equivalence ratio and an exhaust

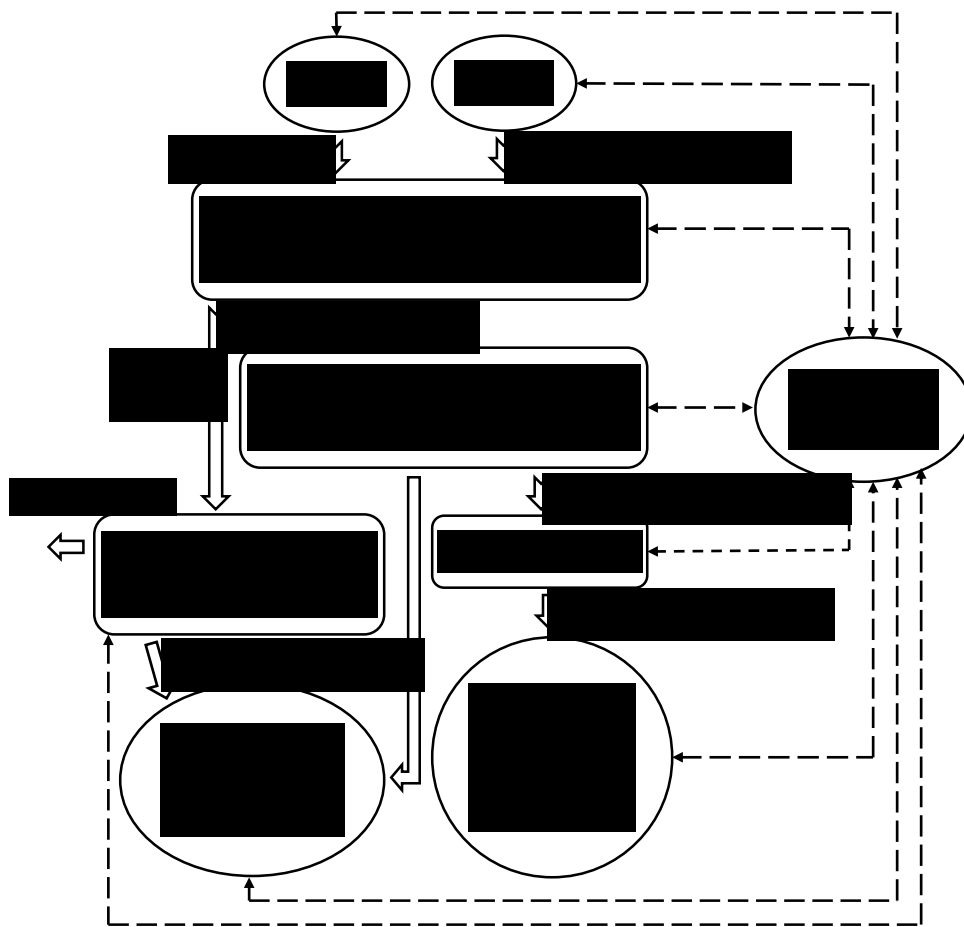


Figure 1-5 WhisperGen MicroCHP control / data transfer

temperature sensor. The engine is also equipped with additional sensors, including thermocouples for inlet air, coolant, etc. and outputs which are logged by the engine's software: Micromon Ver 1.0. Finally, the unit requires servicing every year, or 500 hours of operation, whichever is first [21].

1.4 Literature Review

WhisperGen MicroCHP systems have been tested around the world by many researchers and following are some published results:

Bell et. al [23, 24, 25] published reports on the integration of an early model of the Whisper Tech Stirling engine CHP system into a test house. These papers call for more optimization of the heat recovery system and indicate that on annual basis, the average electrical efficiency was 9%. Later, some field trials were conducted in Europe [26, 27, 28, 29]. Furness in 2007 [30] developed a renewable bio-oil and successfully tested it in a WhisperGen with a slight modification of the combustion chamber.

Professor Murray J. Thomson's combustion laboratory at the University of Toronto experimentally analyzed this engine fueled by diesel, biodiesel, and ethanol on the basis of energy and exergy efficiency [31, 32, 33, 34]. Operation with diesel resulted in power and thermal efficiencies of 11.7% and 78.7%, respectively. No modifications were required for conversion to bio-diesel, and efficiencies were reported as 11.5% power and 77.5% thermal, slightly lower than diesel. With a modified combustion chamber on the same engine, they compared efficiency and emissions running on diesel and ethanol (EtOH), and this resulted in efficiencies of 11.7% power, and 73.7% thermal with EtOH.

Experimental testing was performed, especially to study the effect of coolant on thermal and electrical performance in order to develop and improve a generic Stirling simulation model based on TRNSYS [35, 36]. This model was easily adaptable to WhisperGen and wide range of commercial Stirling engines. Similar researchers [37, 38, 39, 40] have developed empirical equations for different system characteristics (start-up, continuous operation and shutdown) using measured performance data. The model was implemented using MATLAB. Gopal et al. [41] designed and developed a test rig to evaluate the performance of a WhisperGen Stirling Engine. This allowed them to study

displacer lead or lag relative to the power piston, which can be non-sinusoidal and increase the area enclosed in PV diagram, resulting in greater power output.

Pourmovahed et al. [42] used a similar model of a WhisperGen fueled by natural gas, to operate on biogas with no modifications. For the same fuel flowrate, biogas produced 6% and 65% power and thermal efficiencies, respectively and this is significantly lower than natural gas. Later, the economic feasibility of a Stirling MicroCHP was carried out based on results obtained from simulations, taking into account the regulations and economic framework, particularly fuel and electricity prices [43, 44, 45, 46]. Improved dynamic model of a Stirling engine and performance analysis was presented by Cacabelos et al. [47]. They presented a transient model that reproduces experimental behavior when air mass flows were changing. Finally, numerical pressure drop and heat transfer characteristics of a Stirling engine regenerator were analyzed by Costa et al. [48].

1.5 Objectives

Stirling engine based cogeneration systems have many advantages over conventional heat and power; however, many of the operating variables effect on Stirling engine performance are not studied. To make a contribution towards this missing work, the current research is distinguished by three parts:

- Commissioning of a 12 V DC WhisperGen MicroCHP experimental setup fueled by no. 2 diesel for testing Stirling engine, with electrical storage and instrumentation to provide measurements leading to performance analysis.
- Performing a parametric study on primary engine parameters, including air, diesel, coolant flowrate and corresponding temperatures, to further understand their effect on engine power and efficiency.
- Developing a thermodynamic model based on an energy balance of the WhisperGen, to compare experimental results.

1.6 Outline of Thesis

The structure of this thesis is as follows: Chapter 1 includes a motivation, and background to the Stirling cycle engine, a brief literature review focused on the

WhisperGen Stirling engine and the research objectives. Chapter 2 starts with thermodynamic model for energy analysis of Stirling engine only and with heat recovery. This section also explains formulation of thermodynamic equations for Stirling cycle and its dimensionless numbers. Chapter 3 covers extensive specification about experimental apparatus setup including calibration, error analysis of data, related DAQ arrangement, and operating procedure. Chapter 4 presents plots of all engine variables, energy balances, efficiencies, and results of parametric study with discussions. Finally, Chapter 5 provides conclusions and recommendations for future work.

CHAPTER 2

THERMODYNAMIC ANALYSIS

2.1 Energy Balance of a Stirling Engine

Figure 2-1 illustrates the generalized energy flows entering or leaving the Stirling engine system. The thermodynamic system under study is enclosed in a control volume. Major inputs and outputs are diesel, air, electric power, and losses.

The process begins with fuel and air entering and reacting in the combustion chamber, where energy released associated with the chemical reaction (oxidation of the fuel) is transformed into electrical power by the Stirling engine generator assembly. The exhaust heat leaves as exhaust loss or passed through the exhaust heat exchanger where air or water recovers some of the heat in the exhaust for preheating ambient air for continuous combustion or for heat recovery to use for space or water heating, acting as MicroCHP.

To evaluate the performance of the Stirling engine, an energy balance is applied to the control volume shown in Figure 2-1, by identifying the energy input and outputs (Equation 2-1). Terms on left hand side represent energy inputs, while those on the right hand side are energy outputs.

$$\dot{m}_D h_D + \dot{m}_A h_A = P_{El} + \dot{Q}_{L.Other} + \dot{Q}_{L.Coolant} + \dot{m}_E h_E \quad 2-1$$

in this equation, h , \dot{m} , \dot{Q} , and P_{El} denote the specific enthalpy, mass flowrate, heat flowrate, and electrical power, respectively. Subscripts D , A , L , and E denote diesel, air, loss, and exhaust respectively.

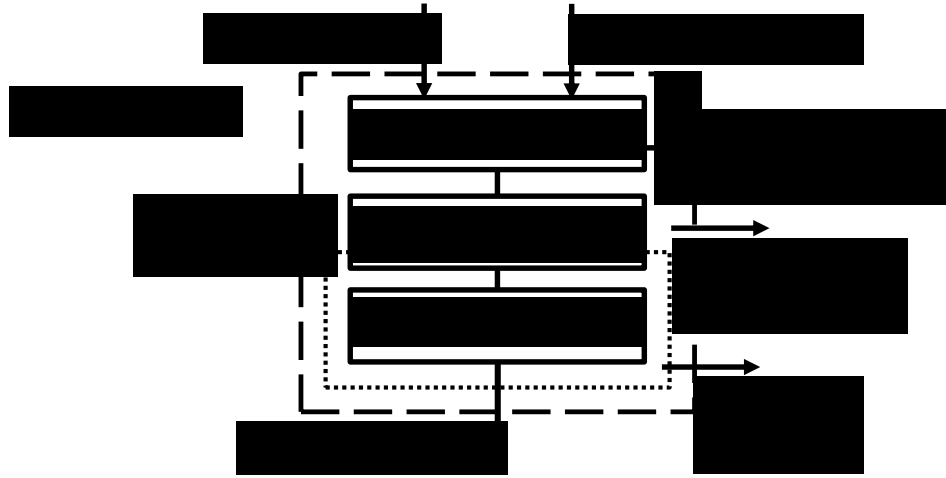


Figure 2-1 Thermodynamic model of Stirling engine system without preheating

2.1.1 Power Efficiency

Electrical efficiency of the WhisperGen is calculated from the above energy balance, as the ratio of net direct current power output from the engine to the net energy content of fuel and air.

$$\eta_{El} = \frac{\text{Electical Output (W)}}{\text{Energy Input (W)}} \times 100(\%) = \frac{P_{El}}{\dot{m}_D LHV_D} \times 100 \quad 2-2$$

where, LHV_D is the lower heating value of the diesel fuel.

2.1.2 Energy Losses

This Stirling engine system has three different heat losses. First is the heat lost in exhaust flue gas ($\dot{Q}_{L,Exhaust}$) exiting combustion chamber (without preheating and heat recovery case), after Stirling engine's utilization for energy conversion. This can be calculated from:

$$\dot{Q}_{L,Exhaust} = \dot{m}_E h_E \quad 2-3$$

Next, heat extracted by the coolant ($\dot{Q}_{L,Coolant}$) from the alternator and cold space of the four cylinders is accounted for in the coolant heat loss (without heat recovery case) from the control volume. Lastly, other energy losses ($\dot{Q}_{L,Others}$), are heat losses to the surroundings from warm surfaces, including the combustion chamber and engine block. Then the total loss from the control volume is:

$$\dot{Q}_L = \dot{Q}_{L.Other} + \dot{Q}_{L.Coolant} + \dot{Q}_{L.Exhaust} \quad 2-4$$

2.1.3 Preheating

A thermodynamic model for preheating is shown in Figure 2-2, where the ambient air is heated by the exhaust flue gas in the exhaust heat exchanger. The preheating can be calculated as

$$\dot{Q}_{Preheating} = \dot{m}_A c_{p.A} (T_A - T_o) \quad 2-5$$

where \dot{m}_A , $c_{p.A}$, T_o , and T_A represent the mass flow rate, specific heat, ambient temperature, and combustion chamber inlet air temperature, respectively.

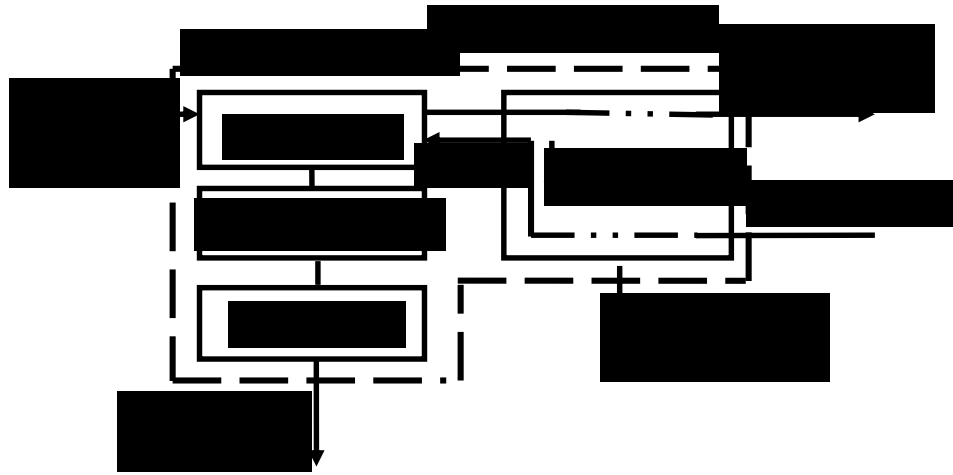


Figure 2-2 Thermodynamic model of preheating ambient air

2.2 Energy Balance with Heat Recovery

This section describes the energy balance of WhisperGen MicroCHP, where the total useful output is calculated from the power and thermal outputs. So, the energy balance (Equation 2-1) is rewritten for the control volume in Figure 2-3, with the addition of thermal output on the left hand side.

$$\dot{m}_D h_D + \dot{m}_A h_A = P_{El} + \dot{Q}_{Th} + \dot{Q}_{L.Other} + \dot{m}_E h_E \quad 2-6$$

The thermal outputs of the WhisperGen system are the heat recovered from the alternator to maintain an uniform low temperature for maximum electrical efficiency, and the heat recovered from the Stirling engine's cold side internal heat exchangers for

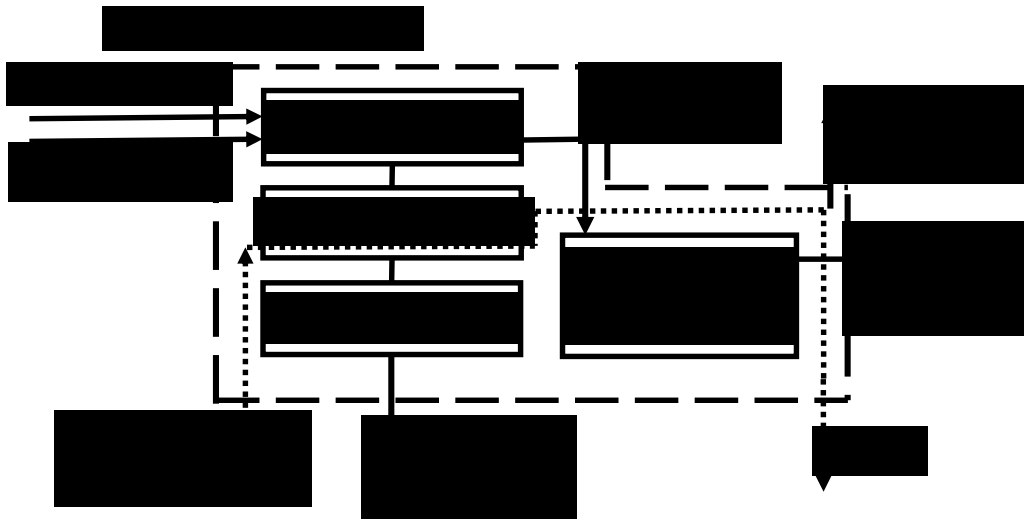


Figure 2-3 Thermodynamic model of Stirling engine with heat recovery

compression work, and the heat recovered from the exhaust heat exchanger as shown in Figure 2-3.

$$\dot{Q}_{Th} = \dot{m}_W c_{p,W} (T_{W.out} - T_{W.in}) \quad 2-7$$

where, $T_{W.in}$ and $T_{W.out}$ are inlet and outlet temperature of water in the heat recovery system, respectively.

The thermal efficiency of WhisperGen system is calculated from thermal output divided by total energy input.

$$\eta_{Th} = \frac{\dot{Q}_{Th}}{\dot{m}_D LHV_D} \times 100 \quad 2-8$$

Finally, the total efficiency of system is sum of all useful output by total input and it is obtained from:

$$\eta_{To} = \frac{P_{El} + \dot{Q}_{Th}}{\dot{m}_D LHV_D} \times 100 \quad 2-9$$

2.3 Stirling Cycle Analysis

The four cylinder alpha Stirling engine's theoretical performance is analysed based on the first law of thermodynamics for the Stirling cycle. P - V and T - S diagrams for the Stirling cycle with imperfect regeneration are shown in Figure 2-4. For simplicity,

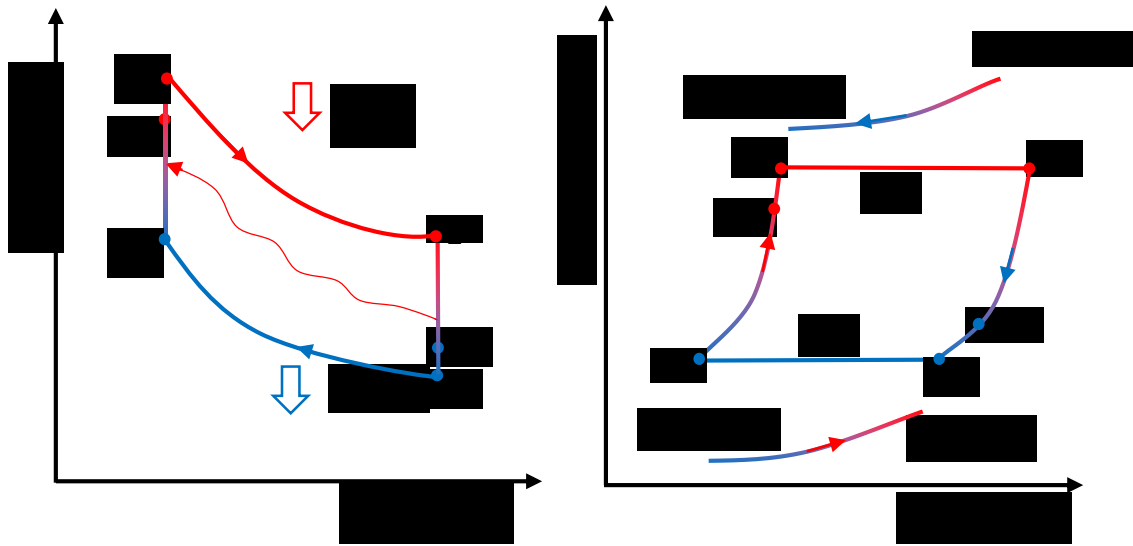


Figure 2-4 P - V and T - S diagrams for Stirling cycle

isothermal operation is assumed in the hot-side heat exchanger, regenerator and cold-side heat exchanger, at temperatures of T_H , T_R , and T_C , respectively at adiabatic conditions (i.e. no heat transfer to the surrounding). The engine is assumed to operate at steady state conditions with a cycle frequency (N) of 1500 RPM. The working fluid is considered to be nitrogen, with the ideal gas assumption, and uniform operational pressure. In our study, Stirling irreversibilities such as dead volumes, imperfect regenerators, cycle internal irreversibility, and convective losses were introduced for a better approximation of the actual WhisperGen Stirling engine power output.

2.3.1 Dead Volumes

The total dead volume of the engine includes dead volumes in the hot space, regenerator and cold space (in m^3) [49]:

$$V_{DT} = V_{DE} + V_{DR} + V_{DC} = (k_{DE} + k_{DR} + k_{DC})V_S \quad 2-10$$

where V_{DE} , V_{DR} , and V_{DC} are dead volumes of heater, regenerator, and cooler volumes respectively, illustrated in Figure 2-5 and Table 2-1. Next, individual dead volumes as ratios of the total dead volume are as follows:

$$k_{DE} = \frac{V_{DE}}{V_{DT}} \quad 2-11$$

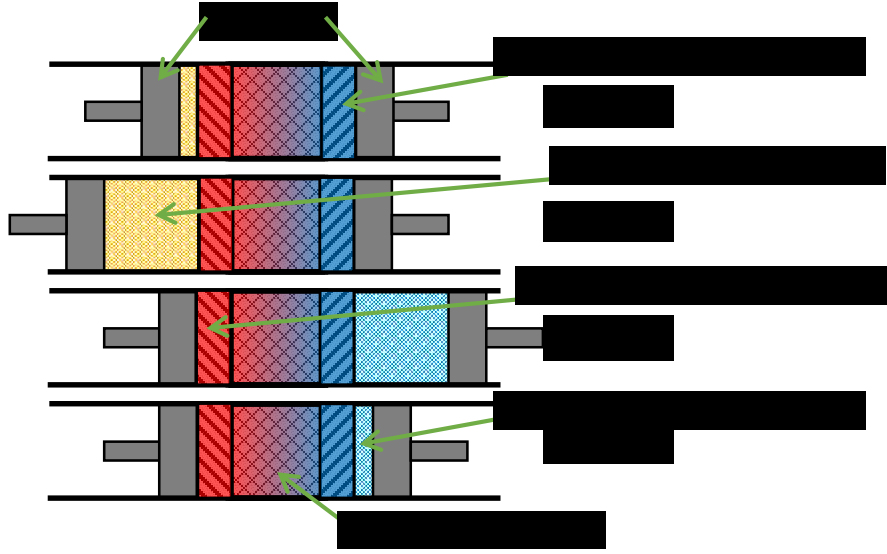


Figure 2-5 State diagram with volumes of Stirling cycle

$$k_{DR} = \frac{V_{DR}}{V_{DT}} \quad 2-12$$

$$k_{DC} = \frac{V_{DC}}{V_{DT}} \quad 2-13$$

where k_{DH} , k_{DR} and k_{DC} are hot space dead, regenerator, and cold space dead volume ratios, respectively. Additionally, the total dead volume to total volume ratio and total dead volume to swept volume ratio can be represented as:

$$k_{DT} = \frac{V_{DT}}{V_T} \quad 2-14$$

$$k_{SV} = \frac{V_{DT}}{(V_E + V_C)} \quad 2-15$$

where V_T , V_E , and V_C are total, expansion and compression volumes, respectively. Then the swept volume, $V_S = V_E + V_C$. Finally, the dead volume contribution is expressed as [50]

$$D = \left(\frac{k_{DE}}{T_H} + \frac{k_{DR}}{T_R} + \frac{k_{DC}}{T_C} \right) \frac{k_{DT}}{1 - k_{DT}} V_S \quad 2-16$$

2.3.2 Regenerator Effectiveness and Temperature

Regenerator effectiveness, ε_R of an imperfect regenerator is defined as the ratio between heat given up in regenerator by the working gas during its passage toward the compression space and the heat received in the regenerator by the working gas during its passage toward the expansion space [51]:

$$\varepsilon_R = \frac{\dot{Q}_{1-1'}}{\dot{Q}_{3-3'}} = \frac{T_{1'}-T_3}{T_1-T_3} = \frac{T_{3'}-T_1}{T_3-T_1} \quad 2-17$$

The value of ε_R is 1 for 100% effectiveness or ideal regeneration and ε_R is 0 for 0% effectiveness or no regeneration. The working fluid temperature at the regenerator outlet can be expressed in terms of regenerator effectiveness as:

$$T_{1'} = T_3 + \varepsilon_R(T_1 - T_3) \quad 2-18$$

Table 2-1 Constants used in Stirling cycle analysis [7, 22, 52]

Description		VALUE	UNITS
Lower Heating Value (diesel)	LHV	42791	kJ/kg
Specific heat at constant pressure (air)	$c_{p,A}$	1009	J/kg·K
Specific heat at constant pressure (nitrogen)	$c_{p,N}$	1122	J/kg·K
Specific heat at constant pressure (water)	$c_{p,W}$	4186	J/kg·K
Gas constant (nitrogen)	R	296.8	J/kg·K
Expansion volume	V_E	3.414E-05	m ³
Compression volume	V_C	2.813E-05	m ³
Regenerator volume	V_R	1.745E-05	m ³
Heater dead volume	V_{DH}	9.180E-06	m ³
Cooler dead volume	V_{DC}	8.269E-06	m ³
Engine speed	N	1500	RPM
Number of cylinders		4	
Total mass of working gas	m	3.750E-04	kg
Conductive coefficient	k_L	2.5	J/K
Specific heat ratio	k	1.4	
Regenerator effectiveness	ε_R	0.62	

For equal heating and cooling regenerator effectiveness, $\dot{Q}_{1-1'} = \dot{Q}_{3-3'}$, and the working gas temperature at regenerator inlet is:

$$T_{3'} = T_1 + \varepsilon_R(T_3 - T_1) = T_1 - \varepsilon_R(T_1 - T_3) \quad 2-19$$

The effective temperature of the working gas contained in regenerator space can be determined using a simple arithmetic mean [51]:

$$T_R = \frac{T_{1'} + T_{3'}}{2} = \frac{T_1 + T_3}{2} \quad 2-20$$

It can be seen that the mean regenerator temperature is not dependent on the regenerator effectiveness.

2.3.3 Irreversibility Parameter

The cycle irreversibility parameter quantitatively describes the effect of internal dissipation of heat on the performance of a heat engine [53]:

$$R_S = \frac{\dot{Q}_H/T_H}{\dot{Q}_C/T_C} \quad 2-21$$

2.3.4 Conductive Loss

The conductive thermal bridging loss value is proportional to the temperature difference from the heat source to the heat sink:

$$\dot{Q}_L = k_L(T_{Source} - T_{Sink}) \quad 2-22$$

where, k_L is the conductive thermal bridge loss coefficient and the value is considered as 2.5 (W/K) [52].

2.3.5 Cyclic Processes

Isothermal Expansion Process: Heat added to the cycle during the isothermal expansion process 1 – 2 is the direct result of expansion work over a range of expansion volumes. So, the hot side working gas volume changes from $V_1 = V_E + DT_H$ to $V_2 = V_S + DT_H$ and cold space working gas volume, V_C , is 0 throughout this process [51].

$$\dot{Q}_{1-2} = \dot{W}_{1-2} = \int_{V_1}^{V_2} Np dV_E \quad 2-23$$

$$= \dot{m}RT_H \ln \left(\frac{V_S + DT_H}{V_E + DT_H} \right) \quad 2-24$$

It is evident that expansion work is dependent on mass, heater side temperature, and dead volume.

Isochoric Cooling Process: In principle, heat rejected during the isochoric cooling process 2 – 3 is:

$$\dot{Q}_{2-3} = mc_v(T_C - T_H) \quad 2-25$$

where c_v is specific heat at constant volume, and is assumed to be constant. Without regeneration, this amount of heat is rejected to the external sink, and for ideal regeneration this amount of heat is absorbed by regenerator. For imperfect regeneration, heat absorbed by the regenerator during process 2 – 3' and heat rejected to an external sink during process 3' – 4 are [51]:

$$\dot{Q}_{2-3'} = \varepsilon_R mc_v(T_C - T_H) \quad 2-26$$

$$\dot{Q}_{3'-3} = (1 - \varepsilon_R) mc_v(T_H - T_C) \quad 2-27$$

It can be seen that heat transfer in the cooling process depends on regenerator effectiveness, mass, and temperatures.

Isothermal Compression Process: Heat rejected during isothermal expansion process 3 – 4 is the result of compression work over range of compression volumes. So, the cold side working gas volume changes from $V_3 = V_S + DT_C$ to $V_4 = V_C + DT_C$ and hot space working gas volume, V_E , is 0 throughout this process [51].

$$\dot{Q}_{3-4} = \dot{W}_{3-4} = \int_{V_3}^{V_4} NpdV_C \quad 2-28$$

$$= mRT_C \ln \left(\frac{V_C + DT_C}{V_S + DT_C} \right) \quad 2-29$$

It should be noted that compression work depends on mass, cooler side temperature, and dead volume.

Isochoric Heating Process: Heat added during the isochoric heating process 4 – 1 is:

$$\dot{Q}_{4-1} = mc_v(T_H - T_C) \quad 2-30$$

Without the regenerator, this amount of heat is added solely by the external source and for ideal regeneration, this amount of heat is released from the regenerator. Then, regeneration heat released from imperfect regenerator during process 4 – 1' and the remaining heat added from the external heat source during process 1' – 1 are [51]:

$$\dot{Q}_{4-1'} = \varepsilon_R m c_v (T_H - T_C) \quad 2-31$$

$$\dot{Q}_{1'-1} = (1 - \varepsilon_R) m c_v (T_H - T_C) \quad 2-32$$

It can be seen that heat input in this heating process depends on the regenerator effectiveness, mass, and temperatures.

2.3.6 Total Heat Added

The total heat addition of an imperfect regeneration Stirling cycle is given as the sum of two external heat input processes and the convectational loss:

$$\dot{Q}_{In} = \dot{Q}_L + \dot{Q}_{1'-1} + \dot{Q}_{1-2} \quad 2-33$$

$$= \dot{Q}_L + m c_v \left[(1 - \varepsilon_R) (T_H - T_C) + (k - 1) T_H \ln \left(\frac{V_S + D T_H}{V_E + D T_H} \right) \right] \quad 2-34$$

where k is the specific heat ratio and the heat input to the engine depends on mass, regenerator effectiveness, temperatures, and dead volumes.

2.3.7 Total Heat Rejected

The total heat rejection of an imperfect regeneration Stirling Cycle is the sum of three heat rejection processes from cycle to external sink:

$$\dot{Q}_{Out} = \dot{Q}_L + \dot{Q}_{3'-3} + \dot{Q}_{3-4} \quad 2-35$$

$$= \dot{Q}_L + m c_v \left[(\varepsilon_R - 1) (T_H - T_C) + (k - 1) T_C \ln \left(\frac{V_C + D T_C}{V_S + D T_C} \right) \right] \quad 2-36$$

The heat rejected from the engine depends on mass, regenerator effectiveness, temperatures, and dead volumes.

2.3.8 Cyclic Power and Efficiency

The surplus energy of two isothermal processes 1-2 and 3-4 is converted into useful mechanical work; and net work for an imperfect regeneration engine with dead volumes can be determined from:

$$\dot{W}_{Net} = \dot{Q}_{In} - \dot{Q}_{Out} \quad 2-37$$

It is evident that amounts of heat added to each cycle and rejected from each cycle are dependent on the internal irreversibility of the cycle. So work output based on the cycle irreversibility parameter R_S is defined as:

$$\dot{W}_{Net} = (R_S T_H - T_C) m R \ln \left(\frac{V_S + DT_C}{V_C + DT_C} \right) \quad 2-38$$

Finally, the Stirling engine thermal efficiency is derived as ratio of net work output to total heat addition:

$$\eta_{Cycle} = \frac{\dot{W}_{Net}}{\dot{Q}_{In}} \quad 2-39$$

2.4 Non Dimensional Analysis

2.4.1 Beale formula

Beale developed a formula which can approximately calculate the power output of a Stirling engine, using a dimensionless number called the Beale number (B_N) [9]. The engine power output in Watts is:

$$P = B_N p_{mean} V_{SE} f \quad 2-40$$

where p_{mean} , f , and V_{SE} are mean cycle pressure in bar, cycle frequency in Hz, and expansion volume of the power piston in cm^3 . The Beale number can be found in many ways and the simplest approximation was developed by Walker in 1980 [2]. The solid line in Figure 2-6 represents Walker's relationship of the Beale number with the source temperature. The upper dotted line represents the high efficiency line, for well designed engines with low sink temperatures. The lower dotted line represents the moderate efficiency line for less well designed engines with high sink temperatures.

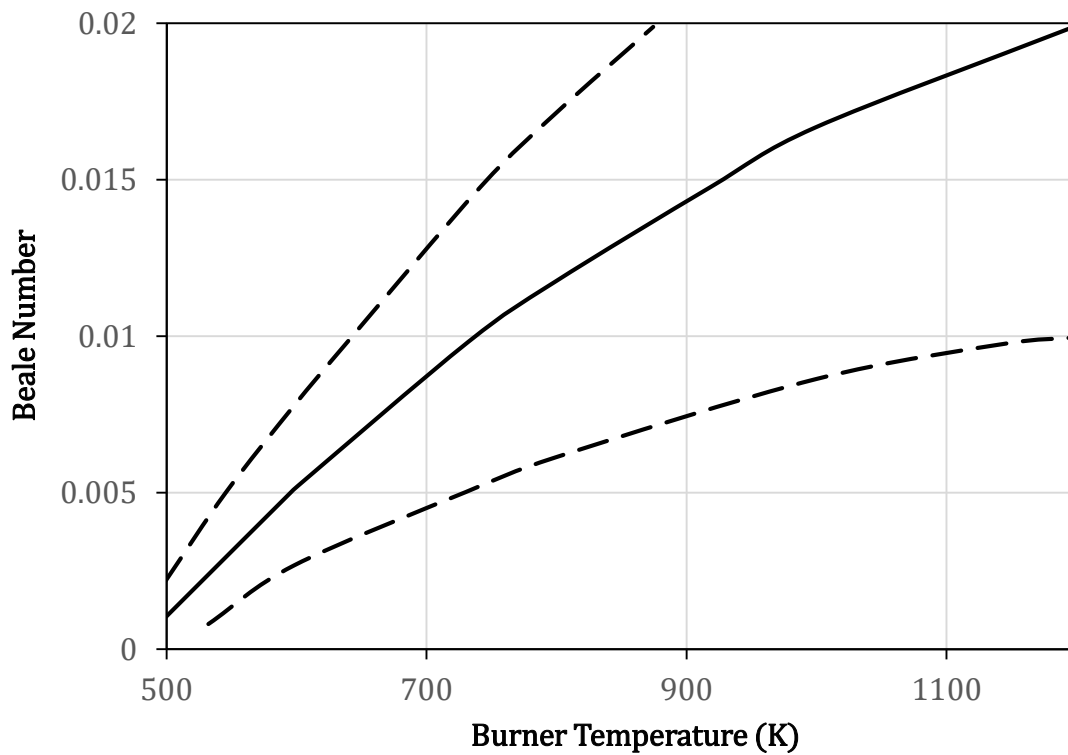


Figure 2-6 Beale number as function of source temperature [2]

2.4.2 West formula

West developed another formula to derive engine power output from engine specifications and new dimensional number called the West number. A key improvement by West is the consideration of temperature effect, as an increase in heater temperature will increase the power at a fixed cooler temperature [11]. The West number is defined as:

$$W_N = B_N \frac{(T_H - T_C)}{(T_H + T_C)} \quad 2-41$$

CHAPTER 3

EXPERIMENTAL METHODOLOGY

In this chapter, the WhisperGen experimental setup is explained in detail along with the description for commissioning each component in the air supply system, fuel system, combustion chamber assembly, exhaust system, cooling system and electrical system. Details of data acquisition systems are also explained with specification of sensors, simple calibration techniques, uncertainty analysis, and respective logging software. Finally, an experiential operating procedure is discussed based on limitations from operational restrictions, and the experimental setup.

3.1 Experimental Installation

The schematic diagram and photograph of the WhisperGen test apparatus detailing electrical and thermal storage are shown in Figures 3-1 and 3-2, respectively. The setup consists of air, fuel, burner, exhaust, Stirling engine, alternator, coolant, heat recovery device, battery, and controller systems or assembly.

3.1.1 Air Supply System

Indoor laboratory air is drawn into the combustion chamber by a 12V DC swirling blower (ebm 12 V G1G126-AB13-56), supplied with WhisperGen. A J-type thermocouple is connected at inlet of air blower to measure intake air temperature. The flow rate of air is measured and controlled using the blower tachometer with an accuracy of 5 l/min using pulse width modulation of the blower fan. The flow range of the blower is 0 – 400 l/min.

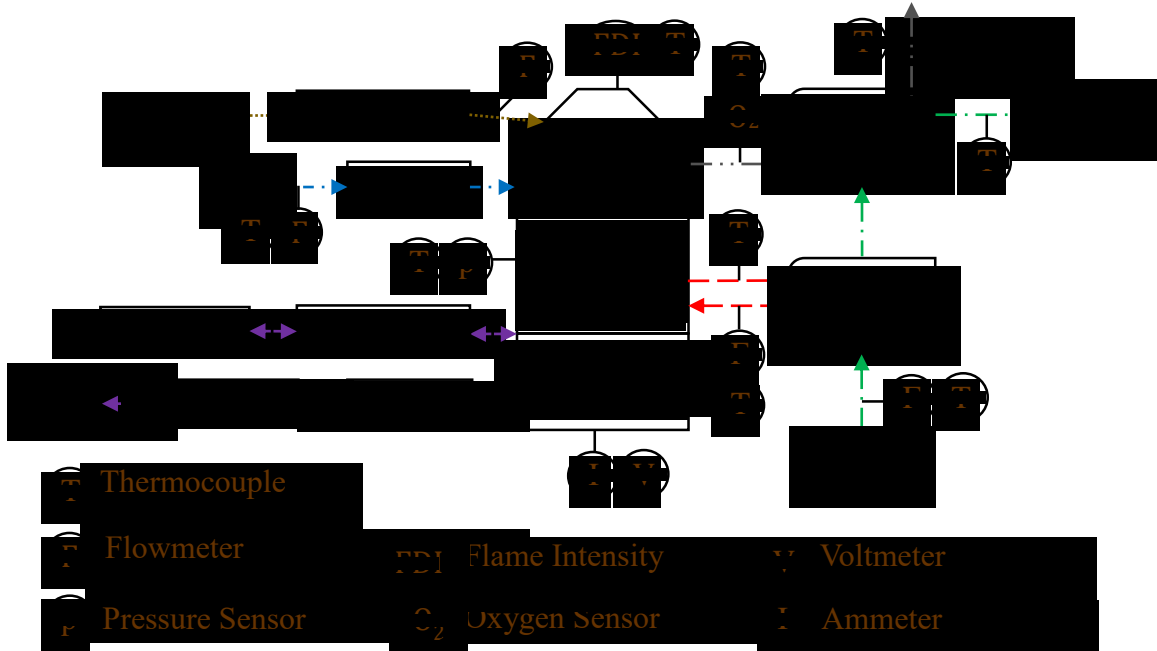


Figure 3-2 Layout of WhisperGen experimental setup

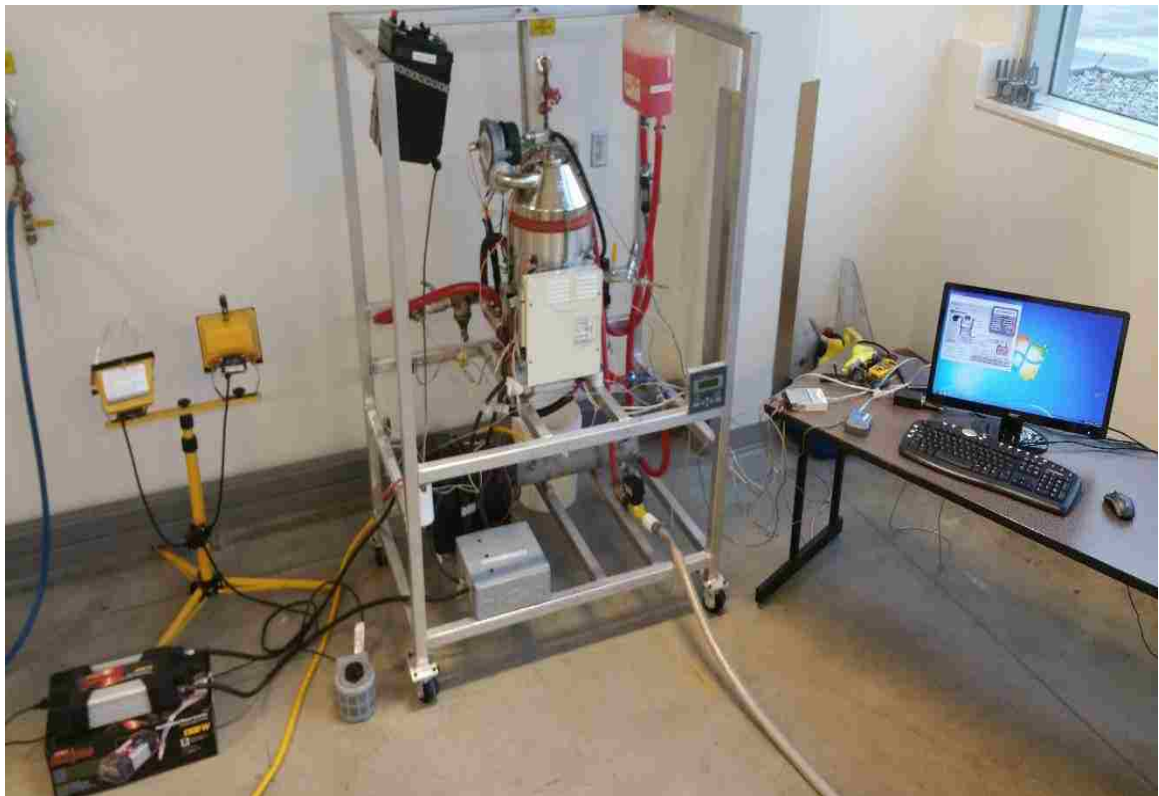


Figure 3-1 Photograph of WhisperGen test setup

3.1.2 Fuel Supply System

The fuel system of the WhisperGen consists of a fuel tank, isolation valves, combined filter / water separator, 12V fuel pump (Mikuni ESP12-MY11A) and interconnecting fuel lines (Figure 3-3). Fuel is stored in one-gallon tank with graduations, to sufficient fuel is available for a whole test. Mechanical and electrical solenoid valves are used for control fuel flow. The pump operates on a pulse width modulated signal from the controller to deliver an accurate amount of fuel into the evaporator. The pump frequency ranges from 0 – 16 Hz and is directly proportional to a fuel flow rate of 0 – 18 ml/min for diesel within 1 ml accuracy.

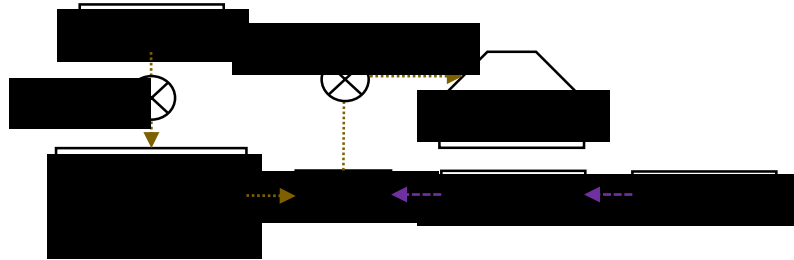


Figure 3-3 Layout of fuel delivery system

3.1.3 Burner Assembly

The WhisperGen burner is a complex unit consisting of a series of sheet metal shells welded concentrically to one another (Figure 3-4). In each sheet metal shell, either fresh air or exhaust flue gas flows in an alternating pattern. By having alternating flow in each cavity, the burner acts as a heat exchanger for cooling the exhaust gas and preheating incoming combustion air. The combustion chamber is placed right above the Stirling engine and is sealed off with high temperature ceramic sealant (McMaster-Carr P.N. 88285K2 and 93435K43). K-type thermocouples are inserted to measure flue gas entering the hot end fin heat exchanger of the Stirling engine (Figure 3-5) and the interface between the burner and the exhaust heat exchanger.

A low noise evaporator is fitted on top of the burner and consists of fine mesh to filter unburnt fuel, a glow plug to preheat the combustion chamber for fuel vaporization, and a flame ionization detector (FID) to detect flame intensity. The evaporator's job is to premix fuel with swirling air and charge the combustion chamber, where it burns as flat

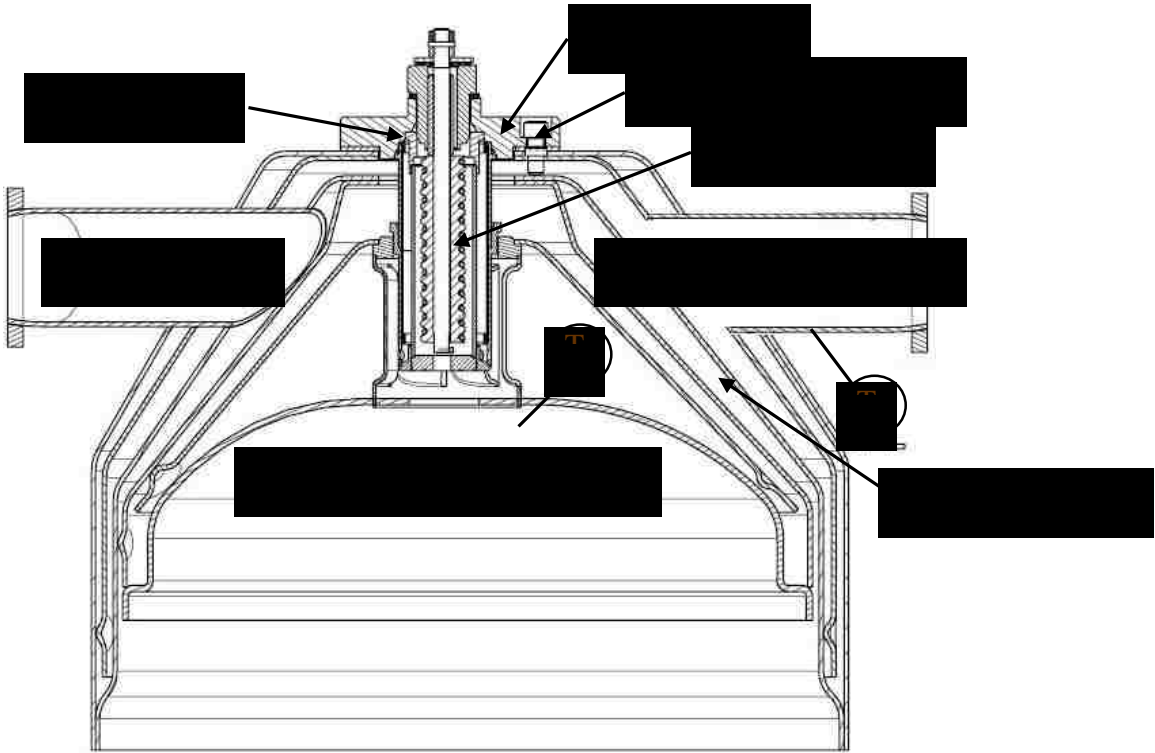


Figure 3-4 Schematic of burner assembly [34]



Figure 3-5 Photograph of internal heat exchanger

sheet due to recirculation created by the diffuser effect of the sudden expansion and vortex breakdown of the swirling flow.

3.1.4 Exhaust System

The exhaust system mainly consists of an exhaust heat exchanger, condensate drain, exhaust tubing, and draft fan. Flue gas flows through variety of tubing, including (30 cm) of rubber hose, (4.6 m) of galvanized steel duct hose (McMaster–Carr P.N. 54945K76) and additional pipe fittings like flanges and elbows. For laboratory safety, the exhaust flue gas is connected to an exhaust pipe from the combustion chamber to the discharge point in the fume hood, without any leakage. A portion of the exhaust is diverted to an oxygen sensor fitted above the exhaust heat exchanger before it enters the condenser. The cooled exhaust temperature is measured using J-type thermocouple fitted on a heat exchanger just above the water trap, which holds condensed water vapour. After exiting the water traps, flue gas is discharged into a fume hood. The WhisperGen can withstand maximum back pressure of 67 Pa at an exhaust temperature of 70°C. So a draft fan is used to reduce the pressure slightly below atmospheric, to prevent exhaust leakage and heat balance change.

3.1.5 Cooling System

The primary cooling system incorporates a header tank, 12V DC coolant pump (WhisperGen P.N. ELPU30175), filter / strainer, and 12V clamp element heater (built into coolant circuit to provide additional heating in certain modes of operation). The primary coolant is 50 % glycol and 50 % water premixed for heavy duty antifreeze in diesel engines with aluminium metal (Canadian tire P.N. 29-3052-2). The coolant line is also fitted with a flowmeter (GPI P.N. A109GMN100NA1), mechanical valve and pressure relief valves to monitor and control coolant flow and pumping flow rate ranges from 6 - 11 l/min. The coolant circuit is also fitted with two J-type thermocouples to measure inlet coolant temperature (fitted before the clamp element) and outlet coolant temperature (at the exit of the engine block) as shown in Figure 3-6. Finally, heat is dumped into the water in the secondary heat exchanger (Seakamp P.N. SK317HU).

The secondary cooling circuit consists of a copper multiple pass shell and tube heat exchanger with an 8 cm diameter and 50 cm length, which removes thermal output from

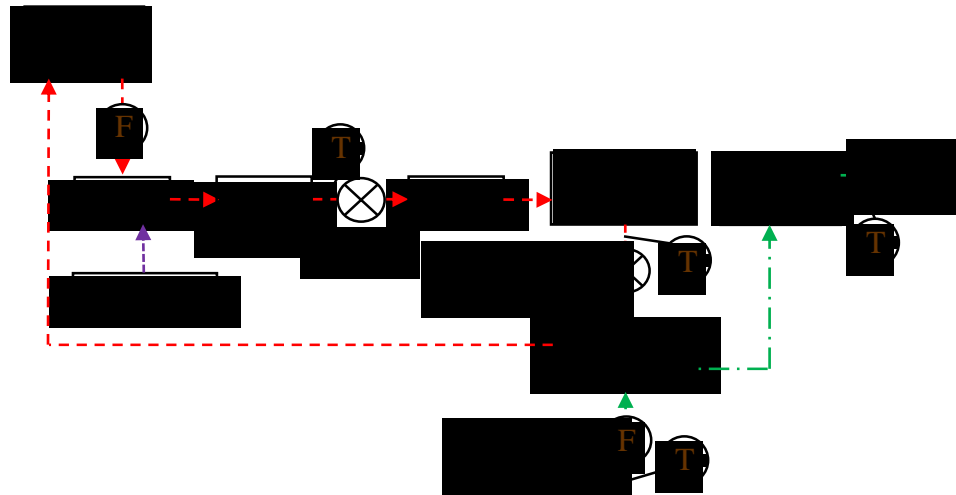


Figure 3-6 Layout of cooling system

the primary engine coolant by running cold laboratory water through the shell in a counter-flow arrangement. Then, it passes through the coolant passage of the exhaust heat exchanger to recover heat from the exhaust flue gas. Two J-type thermometers measure inlet water temperature before the secondary heat exchanger, and the outlet water temperature after the exhaust heat exchanger and rotameter (Omega P.N. FL7303). The maximum flowrate of water is 20 l/min and is controlled by a manual valve.

3.1.6 Electrical System

AC electricity produced by 3 phase alternator is converted into DC by series of rectifiers and is stored in a 650A Nautilus 12V deep cycle lead acid battery (Canadian tire P.N. 10-2493-0). A standard battery was chosen because it is readily available, has enough current to start the engine, and can be used for several other applications. A 1500 W MotoMaster inverter (Canadian tire P.N. 11-1866-8) is used to convert DC electricity into standard 120V AC power. For the purposes of this study, the inverter powers two 500 W portable work lights controlled by a variable resistor (variac) to create a steady state load.

Figure 3-7 shows the WhisperGen microcontroller, battery bank, and electrical load, which are directly connected to the engine with 35 gauge cables for high current up to 100A and the engine chassis is connected to the common electricity ground.

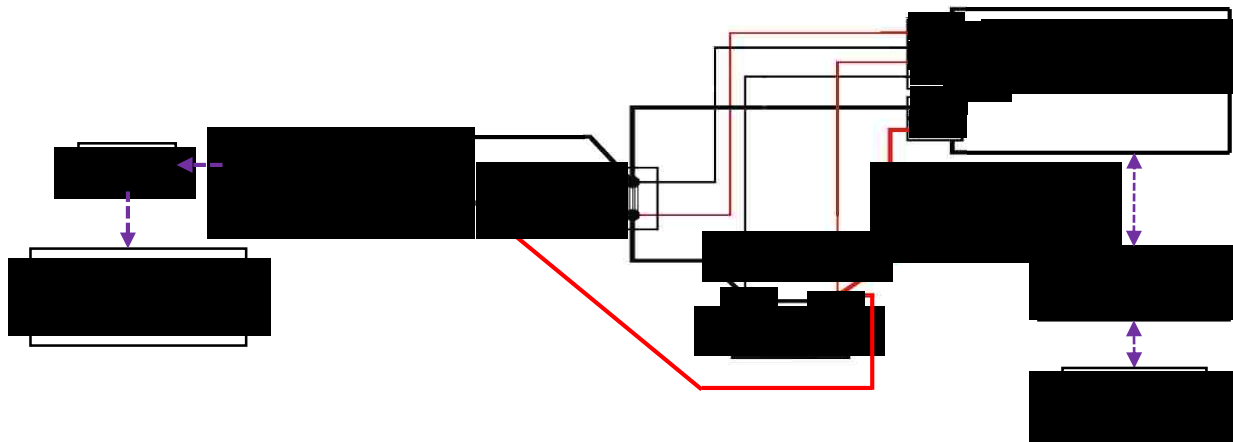


Figure 3-7 Schematic of electrical system

3.2 Data Acquisition System

Sensor installation strictly follows the wiring diagram and specifications given by WhisperGen user’s manual [21] or the circuit diagram supplied by National Instruments (NI) DAQ system, to avoid any electrical damage and inaccuracy in reading signals. The locations of WhisperGen original sensors, additional pressure, temperature, and flow meter are shown in Figure 3-1. Real time data are acquired using the WhisperGen microcontroller, which measures data from several preinstalled sensors and the NI DAQ system measures data from all additional thermocouples and pressor sensors. Both DAQ systems and high accuracy sensors are capable of readings and recording data at 1 second intervals, to capture the transient nature of system parameters.

3.2.1 Sensors

3.2.1.1 Temperature Sensor

In order to increase the accuracy of flow control and heat balance calculations, six additional thermocouples were installed, in addition to the original WhisperGen temperature sensors and switches. The list of thermocouples spread across the test setup is shown in Table 3-1. J-type thermocouples with grounded junctions (Omega P.N. TC–J–NPT–G–72–SMP) were utilized to measure ambient, inlet air, coolant inlet, coolant outlet, water inlet, and water outlet temperatures. These thermocouples feature a 6.35 mm diameter stainless steel sheath and are accurate to approximately ± 0.3 K for moderate

temperature measurements. K-type thermocouples (Omega P.N. TC-K-NPT-G-72-SMP) were used for burner and exhaust temperature measurements, due to their high accuracy (± 0.1 K) and larger temperature range.

Table 3-1 Temperatures measured and instrumentation

Temperature parameter	Symbol	Data logger	Thermocouple type
Ambient air	T_0	LabVIEW	Omega J-type
Inlet air	T_A	Micromon	Omega J-type
Burner	T_B	LabVIEW	Omega K-type
Burner exit	$T_{E.in}$	Micromon	Omega K-type
Exhaust HX exit	$T_{E.out}$	LabVIEW	Omega K-type
Inlet coolant	$T_{C.in}$	LabVIEW	Omega J-type
Outlet coolant	$T_{C.out}$	Micromon	Omega J-type
Inlet water	$T_{W.in}$	LabVIEW	Omega J-type
Outlet water	$T_{W.out}$	LabVIEW	Omega J-type

3.2.1.2 Flame Ionization Detector

A flame ionization detector (FID) is an instrument that measures the concentration of organic ions in a gas stream and is attached to the evaporative burner. The controller uses this signal to predict the flame intensity in the combustion chamber, which is required for stable combustion. After engine testing, it was found that the flame rod signal varies from 0 to 10 μ A and is linearly related to the exhaust temperature signal and increases with flame intensity.

3.2.1.3 Oxygen Sensor

The oxygen sensor (Honeywell P.N. OXY6200) features two zirconium dioxide (ZrO_2) discs with a small hermetically sealed chamber in between. One of the ZrO_2 discs

acts as a reversible oxygen pump, which is used to fill and empty the sample chamber. The second disc then measures the ratio of the partial pressures and generates a signal which is read by the engine control system. In order to obtain the required operating temperatures of 927 K for the ZrO_2 to operate as an oxygen pump, a heating element is used. This real-time sensor signal corresponds to the oxygen content in the exhaust, with an accuracy of $\pm 2\%$, and is used to calculate the fuel-air equivalence ratio, assuming complete combustion.

3.2.1.4 Flowmeter

Two high temperature (< 400 K) pulsed output rotary flowmeters were installed to monitor the flow rates of the primary engine coolant and laboratory cold water, respectively. First, the coolant flowmeter (GPI P.N. A109GMN100NA1) is mounted immediately downstream of the primary coolant tank and has an accuracy of $\pm 2\%$ for a flow range of 1 - 11 l/min. Next the flowmeter (Omega P.N. FL7303) monitors the cold water flowing from the laboratory tap and has an accuracy of $\pm 2\%$ for 1 to 18 l/min.

3.2.1.5 Voltmeter and Ammeter

The WhisperGen measures the voltage and current of several electrical components including the alternator, shunt, bus, battery, and external electrical load. Also the net DC electrical output of the Stirling generator assembly is calculated from the voltage across the alternator terminal with an inline fuse (2A), and the current across a 500A, 50mV current shunt connected in series with a 150A circuit breaker.

3.2.2 Sensor Calibration

It is critical to achieve accurate monitoring and data recording for proper performance calculation of the WhisperGen system. Most of the preinstalled sensors in the engine are factory calibrated, leaving only a few thermocouples and two flowmeters to calibrate. Sensors were calibrated with an offline technique, which corresponds to comparing the temperature reading from calibrated sensors and inculcating the differences in the corresponding DAQ system [54]. This calibration method is repeated for flowmeters by timing the flow of a standard volume.

3.2.3 Uncertainty Analysis

To understand the significance of experimental test results, this section outlines the uncertainty calculations recommended by the American Society of Mechanical Engineers and demonstrates error propagation and the relative magnitudes of different sources of error [55]. Uncertainties of measured and derived quantities are calculated from the known or estimated instrument bias error. The measurement instrument's quoted accuracy was used as the bias error when known. But, bias errors of measurements provided by the Stirling engine's commissioning software were unknown, so a bias of 1% was assumed for these variables. Thus, the total bias and standard deviation for each measured parameter, x , at a recorded data interval, i , is calculated as the sum of the squares of bias error components for that measurement:

$$B_x = \sqrt{\sum_{i=1}^n B_i^2} \quad 3-1$$

$$S_x = \sqrt{\frac{\sum_{i=1}^n (x_i - x_{avg})^2}{n-1}} \quad 3-2$$

where n , x_i , and x_{avg} are the number of recorded data intervals in the set, measured data at each interval, i , and mean value for the set.

The total uncertainty of a measured quantity is calculated by combining the bias and precision errors:

$$U_x = \sqrt{B_x^2 + (tS_x)^2} \quad 3-4$$

where U_x is the uncertainty for 95% two sided confidence levels, respectively, and t is the Student's t value evaluated as a function of n .

The uncertainty of a derived quantity is propagated via the bias and precision indices of measured quantities presented in Equation 3-1 and 3-2. Finally, a similar equation applies for the total uncertainty:

$$y = f(x_1, x_2, x_3, \dots) \quad 3-5$$

$$U_y = \sqrt{\sum_{i=1}^n \left(U_{x_i} \frac{\partial y}{\partial x_i} \right)^2} \quad 3-6$$

3.2.4 Data Logging Software

In order to monitor and record all relevant data the thermocouples, pressure sensors, oxygen sensor, flame ionization rod, tachometer, flowmeters, voltmeter and ammeter, two logging programs are used: WhisperGen engine software Micromon Ver. 1.0, and LabVIEW 2015.

3.2.4.1 Micromon

The WhisperGen system comes with its own commissioning software Micromon Version 1.0, shown in Figure 3-8. This software is used to log the operations and output of

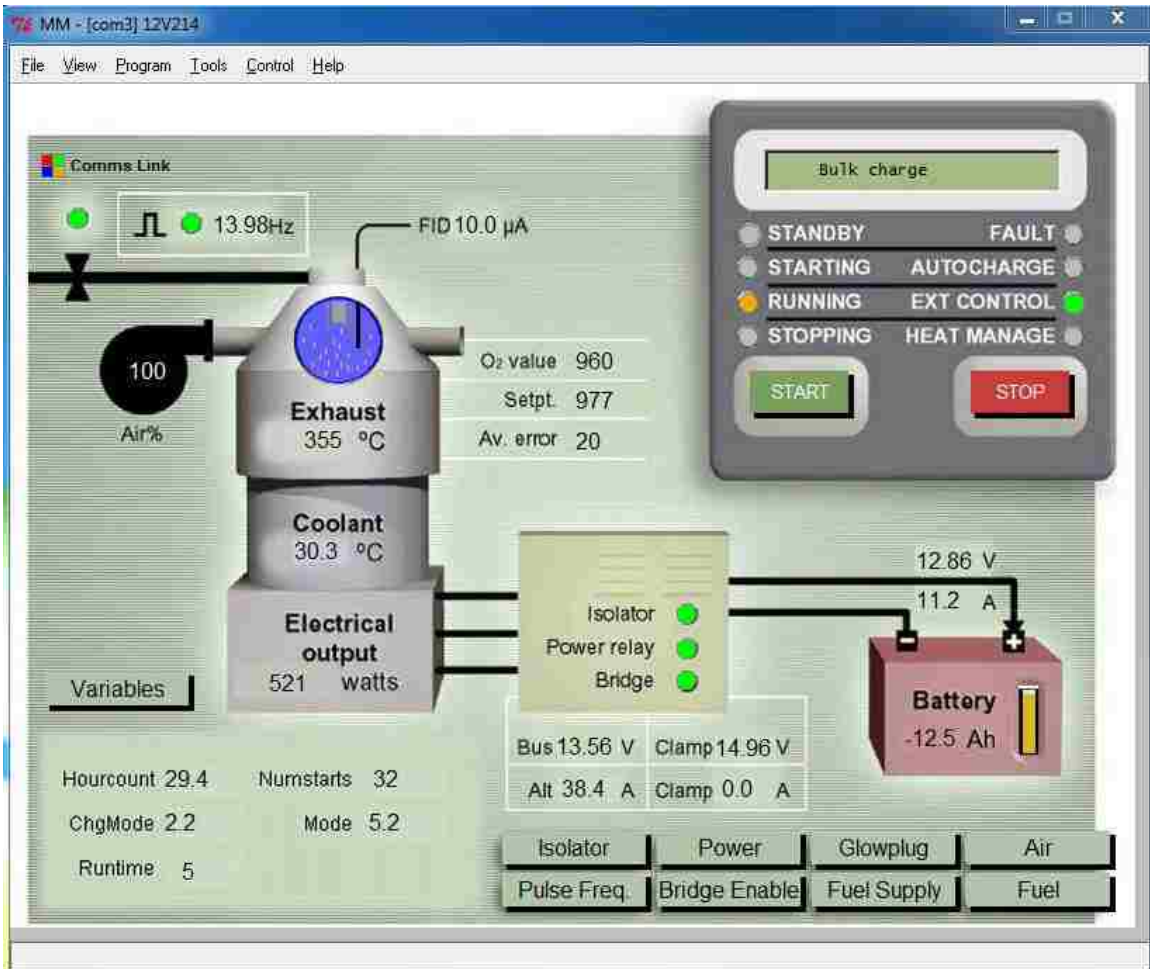


Figure 3-8 Screenshot of WhisperGen control software Micromon

the engine, including the air supply rate, fuel supply rate, glow plug operation, exhaust temperature, coolant temperature, power output, battery voltage, alternator current, stages of operation and many other parameters. This software not only provides the capability to observe and log the engine performance, but also allows the user to adjust various engine operating parameters like temperature set point, oxygen sensor set point, initial fuel flow and glow plug duration for optimizing engine performance.

3.2.4.2 LabVIEW

The LabVIEW 2015 software was used to log real time data from thermocouple module NI 9205 docked in NI cDAQ-9178. This platform consists of block diagrams with controller modules to deduct the voltage signals from the thermocouples and convert them into engineering units. Then, the front panel of the LabVIEW software shows the temperature data in a graphical manner ready to output as data file.

3.3 Operating Procedure

For this study, the engine was operated in maintenance mode, with both auto charge and heat mangle off, which override the battery management function and produced the maximum amount of power. The tests are commenced with maximum run hours set as 1, enough for laboratory testing. When the start signal was received by the engine's controller, a sequence was initiated and it is shown in Figure 3-9. Part of this sequence are tests to ensure all the electronic parts are functional, for example the glow plug is tested by switching both the power and isolator relays on and monitoring the voltage drop ($< 7V$) in the bus. In the same way, the oxygen sensor is tested for functionality by pumping fresh

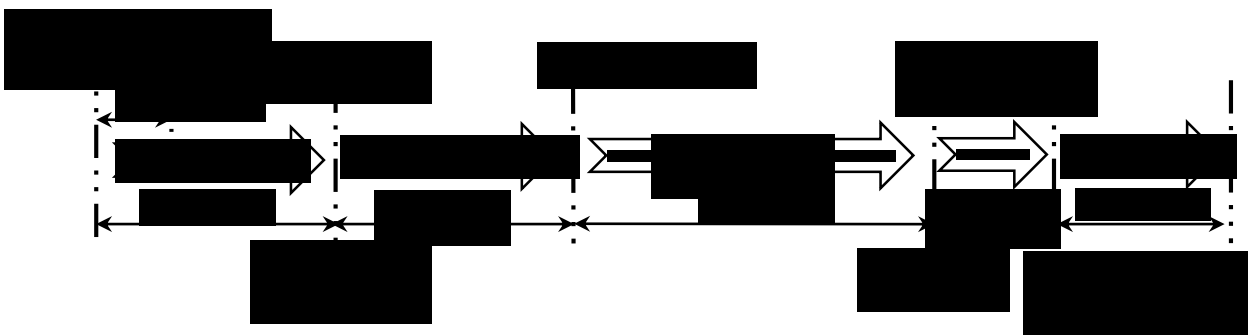


Figure 3-9 Engine test procedure flow diagram

air from the air blower. Immediately after the pretest, the engine's control systems go through the preheat sequence for five minutes where the glow plug is operated to heat the combustion chamber. At any point in the engine operation, if the control system powers down the engine it displays the corresponding error or warning code and when it occurred.

At the five-minute mark, the control system initiates the fuel pump. This builds up flame in the combustion chamber as monitored by the flame rod. In this stabilizing stage the equivalence ratio is slowly increased until the energy input by fuel is about 10 kW. This is again managed by the exhaust temperature and plays a key role in engine operation as it is used by the control systems for cranking the engine during the heat up stage, when to shut off the glow plug, and the amount of air required through the system during the ignition phase.

Similarly, the oxygen value is monitored continuously throughout testing, and the air flow rate is adjusted to keep the equivalence ratio (ϕ) consistent. The engine is cranked at the fifteen-minute mark or at 530 K exhaust temperature. The engine reaches steady state after approximately 10 minutes of operation and the engine was allowed to continuously run for twenty more minutes while the power generation was 1kW. During this steady operation the cooling system was adjusted to maintain the coolant temperature and to recover maximum thermal output. This was done by keeping the secondary cooling circuit temperature as low as 280 K and the corresponding flow rate between 10 – 15 l/min.

The power generation of the WhisperGen system is based on three stages of charging: bulk charging, absorption charging and float charging. In order to evaluate the engine's maximum load performance, the engine must be kept at the bulk charging stage throughout the steady operation. This was accomplished by applying an external load of 1000 W light bulb with an adjustable resistor; maintaining the battery charge at 80%, and ensuring the clamp element was not changing the energy balance.

Following the running stage, when the stop signal is received, the control system stops the fuel supply. Then the air flow rate is decreased for a few minutes, so the working fluid can capture the remaining heat in the combustion chamber and continue to generate electricity for another five minutes. Finally, the alternator stops generating electricity, the

blower forces air through the system at maximum flowrate to cool the engine and to capture the remaining heat through the exhaust heat exchanger.

CHAPTER 4

RESULTS AND DISCUSSION

The main goal of this study was to commission and measure the performance characteristics of the WhisperGen Stirling engine system. Additionally, the engine was analyzed for all operating parameters and the engine performance was calculated. Further, the parametric studies on engine variables like, air flowrate, diesel flowrate, coolant flowrate, inlet air temperature, coolant inlet temperature, and coolant outlet temperature were carried out to study their effect on engine power and efficiency. Finally, the WhisperGen Stirling engine's energy balance was examined with exhaust heat recovery.

4.1 Engine Operation

Performance of the WhisperGen Stirling engine depends on several parameters like air flowrate, diesel flowrate, and various system temperatures and these parameters are time dependent characteristics and take a long time (20 minutes) to achieve steady state.

Air Flowrate (\dot{m}_A): is the flowrate of air from the blower to the combustion chamber and is controlled by the WhisperGen microcontroller. This flowrate varies throughout the engine startup, and shutdown stages, as shown in Figure 4-1. Initially, the flowrate starts at 70 l/min for a quick functionality test of the blower and during the preheating stage for five minutes. Just before the fuel is turned on, the air flowrate hikes to check the operation of oxygen sensor and then the air flowrate is increased to 300 l/min with diesel fuel flow to maintain fuel air equivalence ratio. Later the air flowrate was almost constant around 275 l/min while engine was running, until a stop command was initiated at 45 minutes. At the stop command, the air flowrate was reduced to the minimum, while engine's working fluid, nitrogen, absorbed all the remaining heat from the combustion chamber and then the flowrate was raised to its maximum to cooldown the combustion chamber.

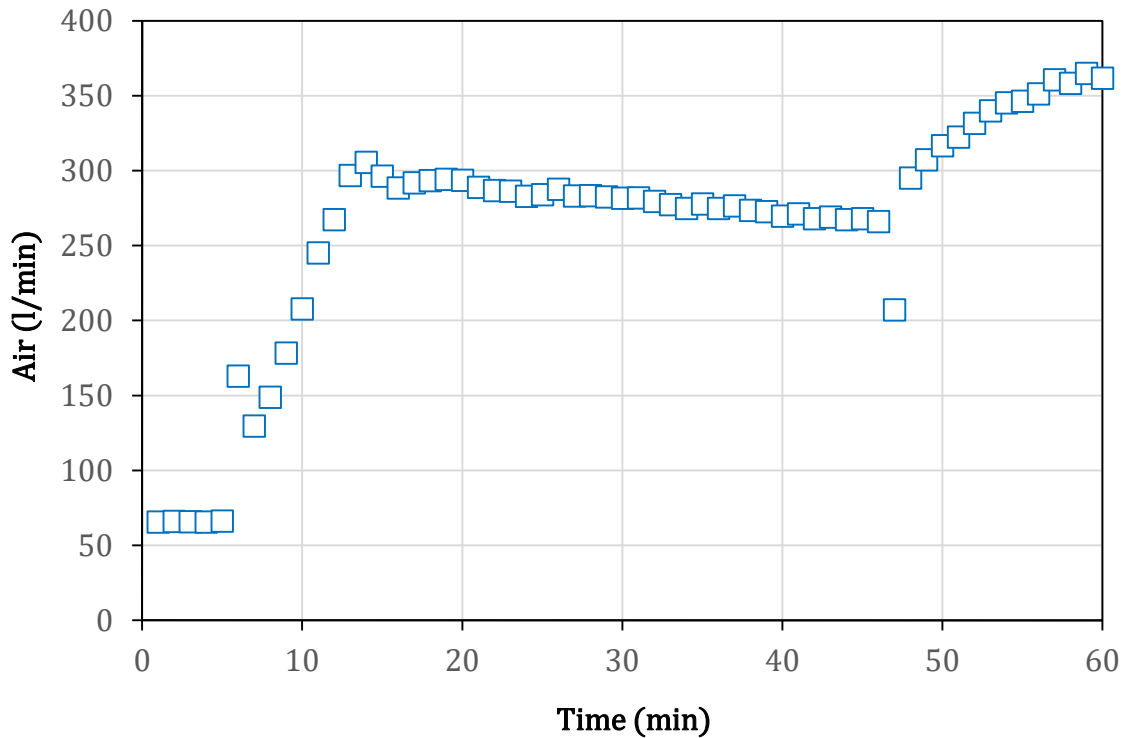


Figure 4-1 Air flowrate

Diesel Flowrate (\dot{m}_D): is the flowrate of diesel fuel to the evaporator for combustion. This flowrate is controlled by the programmed WhisperGen microcontroller and starts when the evaporator is hot enough to evaporate the diesel air mixture for combustion, at around 5 minutes. Initially, the diesel flow started at a low flowrate of about 4.5 ml/min and built up for the required energy input of approximately 10 kW. Then, the high fuel input of 19 ml/min was to boost the temperature of the burner. And then, the flowrate dropped to 17.5 ml/min to maintain the proper fuel-air equivalence ratio during steady state. Finally, as shown in Figure 4-2, the flow was switched off once the stop command was received at the 45-minute mark.

Equivalence Ratio (ϕ): of a system is defined as the ratio of the fuel to oxidizer ratio to the stoichiometric fuel to oxidizer ratio. The equivalence ratio was calculated based on the stoichiometric equivalence ratio of C2 diesel as 14.5. Figure 4-3, shows the equivalence ratio of the combustion process and the initial fluctuation relates to variation of air and fuel

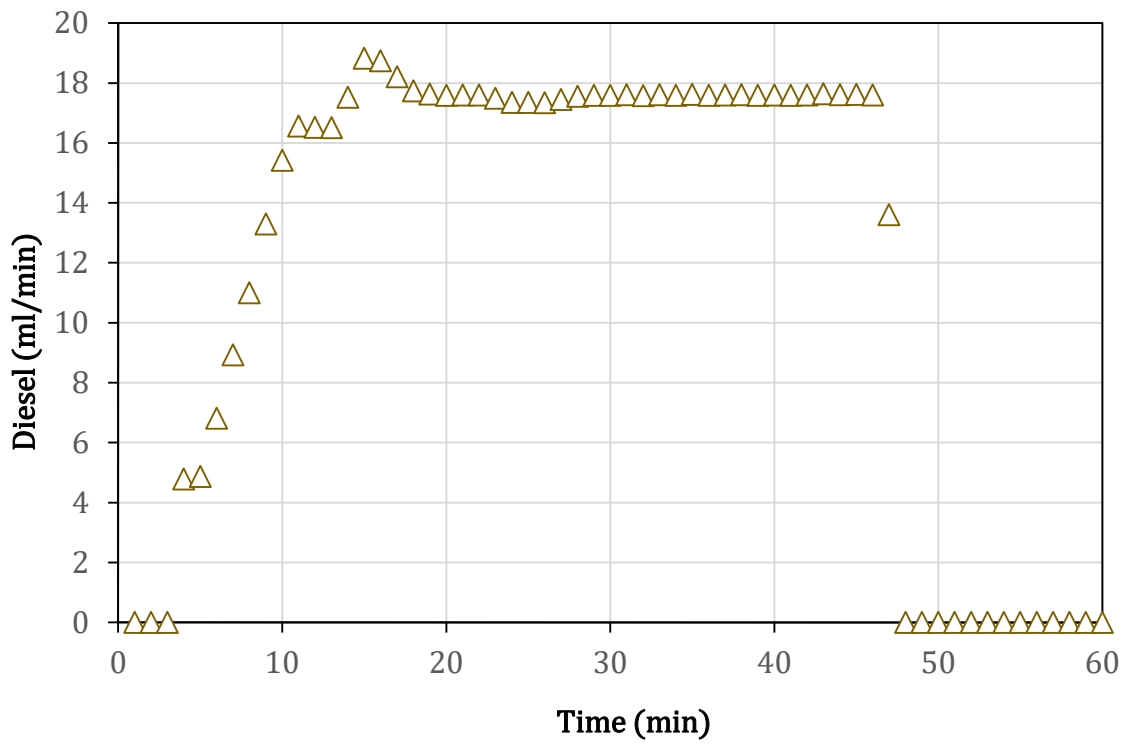


Figure 4-2 Diesel consumption

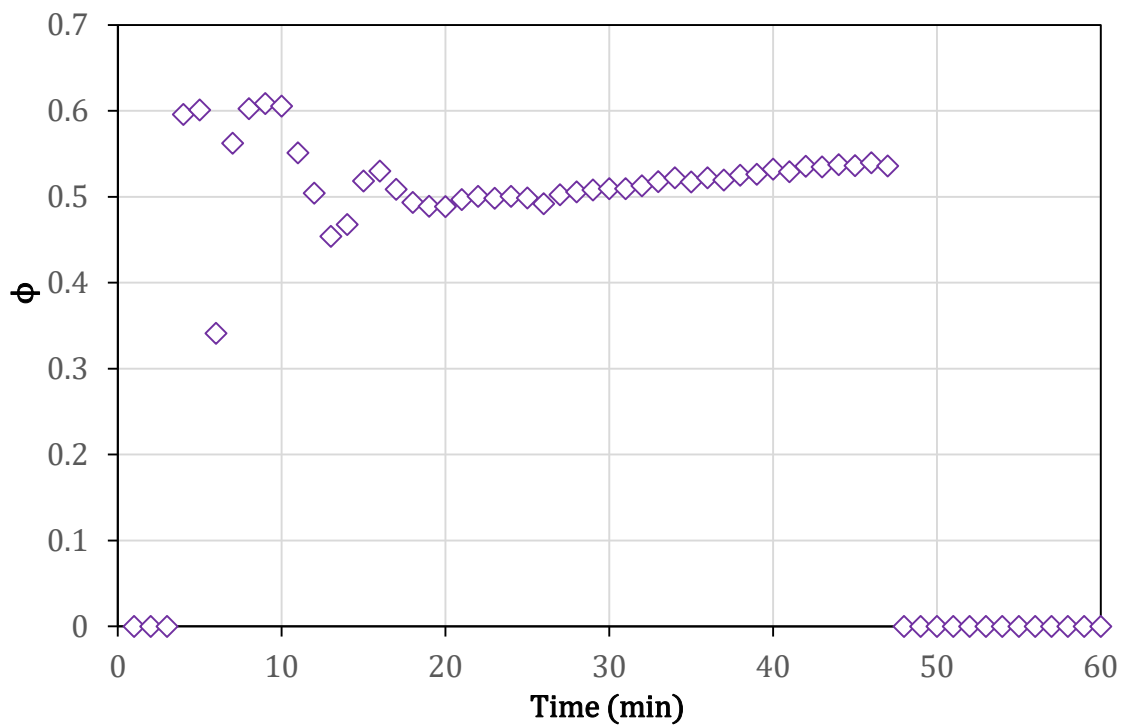


Figure 4-3 Fuel air equivalence ratio

during stabilization. At steady-state, the equivalence ratio was maintained at 0.5 – 0.55 and this clearly shows the system setting for lean combustion.

Oxygen concentration: is the amount of oxygen in the exhaust flue gas and is measured as part per million (ppm). This is shown in Figure 4-4, where it ranges from 750 – 2000 ppm. The value gradually decreases with increase in combustion and is almost stable around 1000 ppm indication equilibrium combustion value. This oxygen value is used to calculate the equivalence ration and can be adjusted for leaner or richer combustion. Finally, it increases with end of combustion at the 45-minute mark and is high due to air flow.

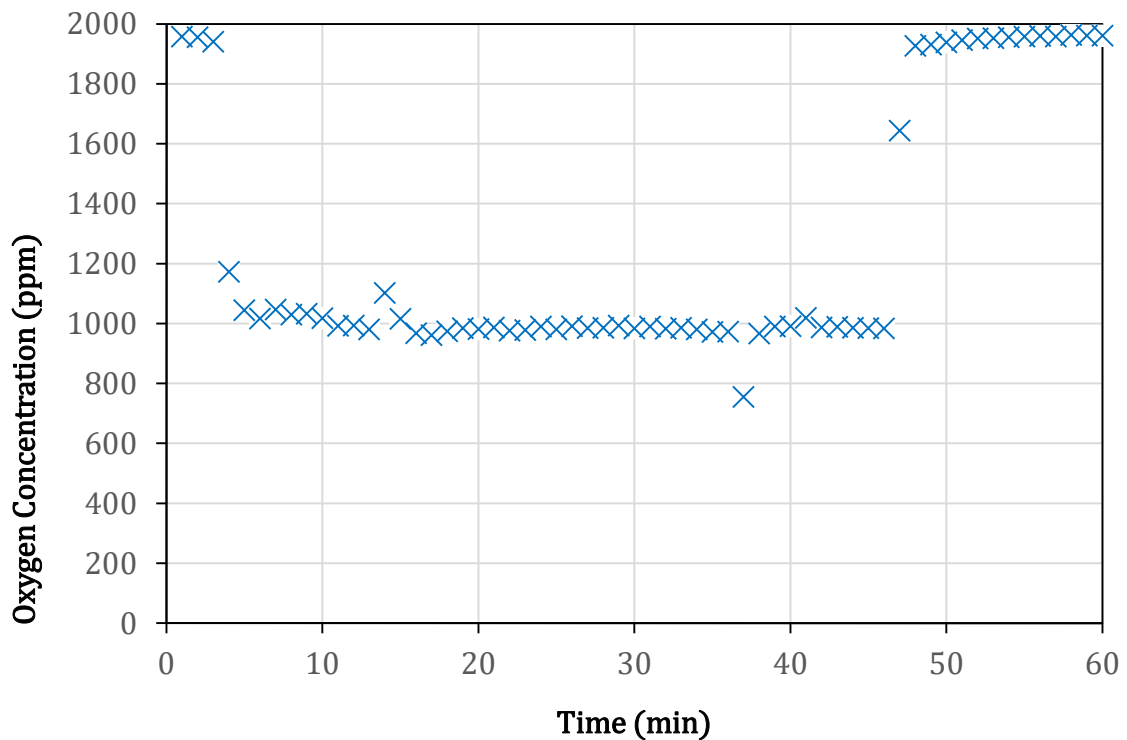


Figure 4-4 Oxygen concentration

System Temperatures: Figure 4-5 shows the variation of ambient air, inlet air, burner, exhaust, coolant inlet, coolant outlet, water inlet and outlet temperatures with time. These temperatures are some of the important parameters which affect the performance of Stirling engine. The graph clearly shows the transient nature of some of the temperatures and the amount of time taken to attain steady state. Starting with ambient temperature (T_0), which

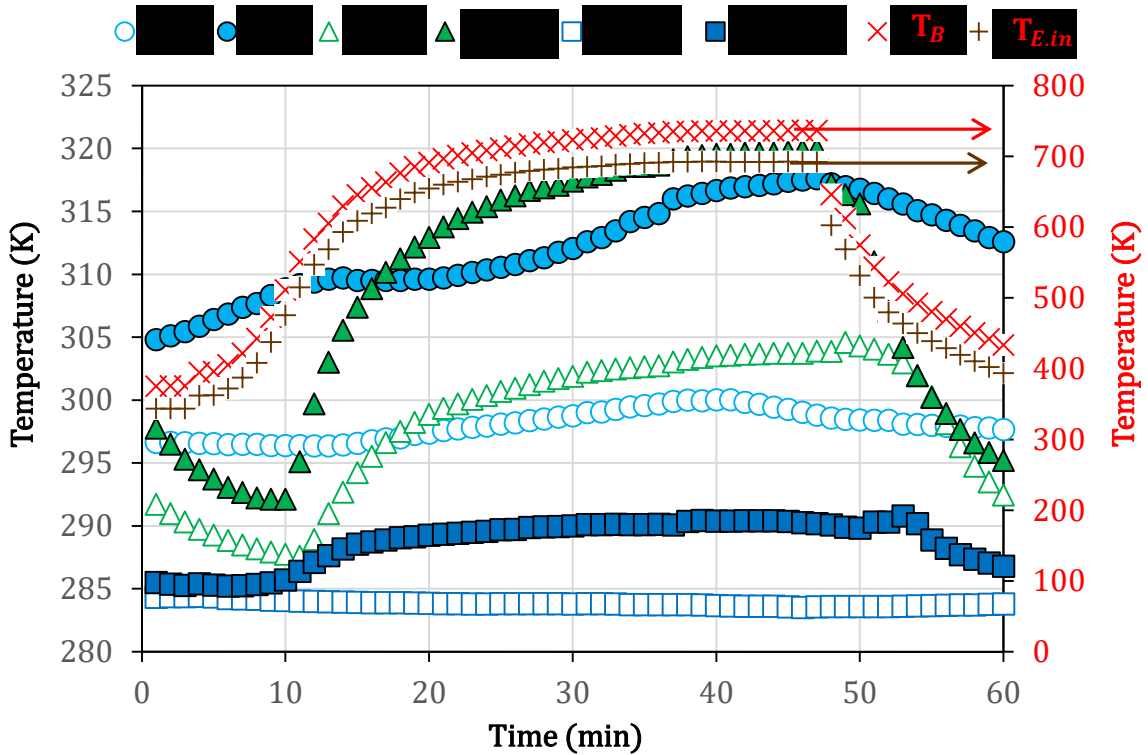


Figure 4-5 System temperatures variation

is the temperature of the surrounding air, or the laboratory temperature. This was initially constant at 295 K and increased slightly to 300 K, due to radiation heat loss from the engine. Then, the inlet air temperature (T_A) was always higher than the ambient, even though the blower took in air from the surroundings. This was due to the higher surface temperature of the engine by convection loss from the combustion chamber and engine block.

The burner (T_B) and exhaust ($T_{E.in}$) temperatures began as low as the ambient temperature and increased rapidly with stabilization of the flame in the combustion chamber. Although both reached about 680 K, they took some time to stabilize to constant values. Later, the temperature decreased when the combustion ended and declines with engine cooldown. A similar trend is found in coolant temperatures ($T_{C.in}$ and $T_{C.out}$) and the temperature difference of the coolant is due to the heat extracted from the alternator and engine block. The initial temperatures decreased from 0 – 10 minutes is due to the cooling of the coolant with no thermal output from the engine. Towards the end, the

increase in water outlet temperature ($T_{W.out}$) was due to thermal extraction from the secondary and exhaust heat exchanger and varying water inlet temperature ($T_{W.in}$) shows the transient nature of the laboratory cold water

4.2 Engine Performance

WhisperGen's performance depends on both the DC electrical output from the alternator and the thermal output from exhaust heat recovery. The power or electrical output of the Stirling engine starts when the bridge relay is enabled and the engine is cranked at the preset exhaust temperature by the alternator (acts as starter motor). The negative power in Figure 4-6 was due to this cranking action and the fluctuation of power before this (not shown) did not contribute to any power output. Next, during the running up stage, the engine power drastically increased from 650 W to 900 W, with the increase of burner temperature. Then, it slowly increased to the rated power output of 1 kW towards the end of steady-state operation. The power output of the engine might have been slightly lower than on the graph, as the graph does not include power consumed by engine's

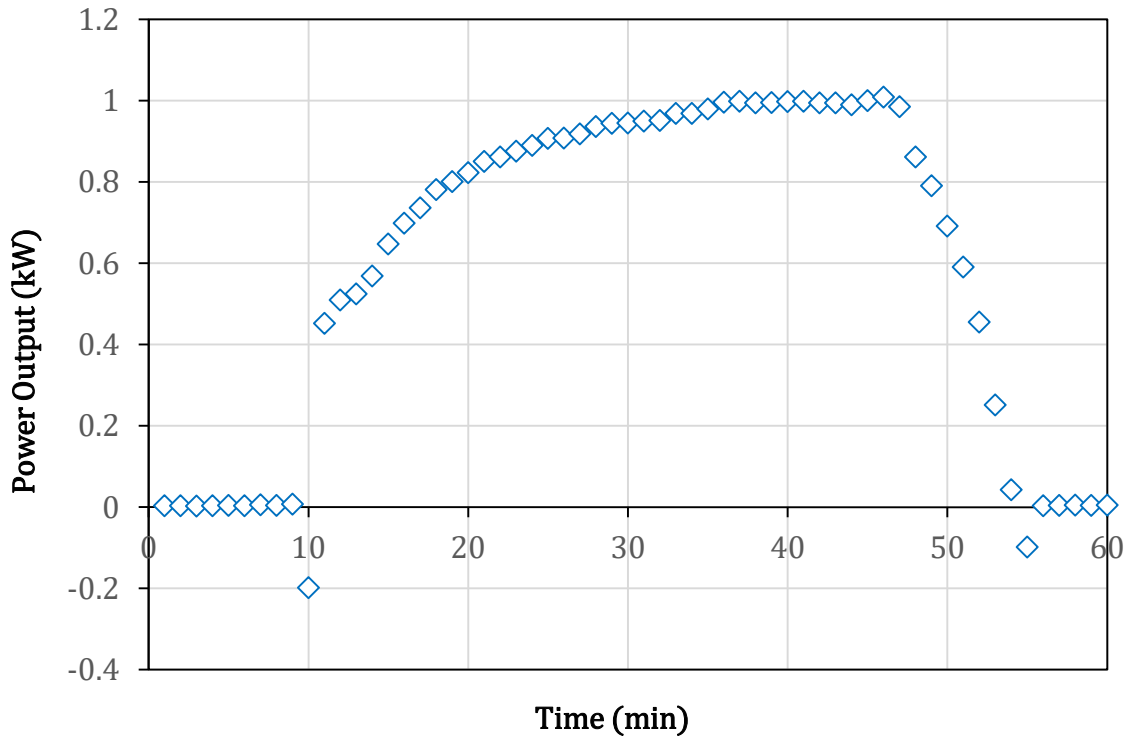


Figure 4-6 Electrical output

electronic components like the coolant pump, air blower, etc. Finally, while in the rundown state, the engine continued to produce power with the remaining heat for about 5 minutes and the engine was stopped with active braking action.

The electrical efficiency of the WhisperGen Stirling engine was calculated from diesel flowrate, LHV of diesel, and power output. The transient nature of the power efficiency is shown in Figure 4-7, where the system achieved a maximum efficiency of 10.5%. The graph also shows the extended amount of time taken by the Stirling engine to reach maximum efficiency. Again, the actual efficiencies will be slightly lower than those reported here, since the power output that is logged by the Micromon software (Figure 3-8) does not account for the power consumption of ancillary components.

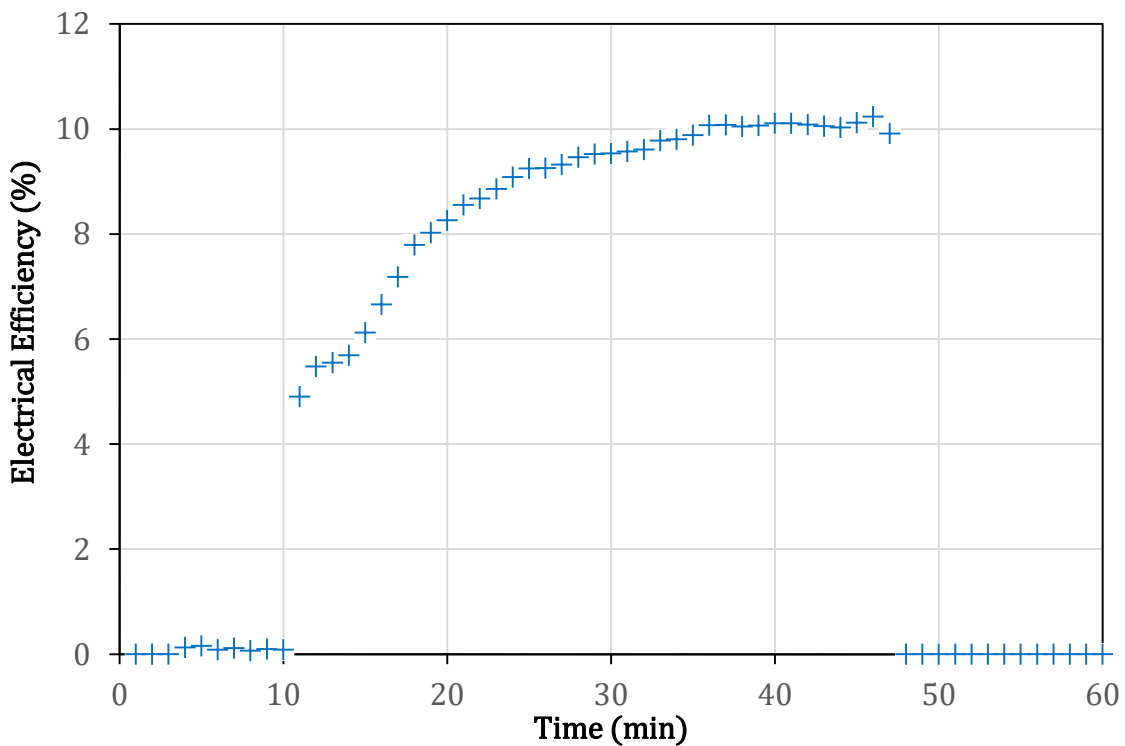


Figure 4-7 Electrical efficiency

4.3 Reproducibility and Uncertainty

Additional tests are conducted to ensure a high level of reproducibility associated with the testing. Table 4-1 lists the steady state engine parameters for a series of tests. All parameters only fluctuate 1% during steady state operation and the results are reproducible.

In summary, a minor increase in air flow and slight reductions in coolant temperature and burner temperature, have a negligible effect on the power output and efficiency. The steady state electrical efficiency and power output for a series of tests, are also reproducible and the average results are quite close. This reproducibility is due to the fact that the engine performance is highly dependent on the fuel flow rate and this is controlled accurately by the controller.

Table 4-1 Engine parameters and performance for multiple tests

Experiment	\dot{m}_A (kg/hr)	\dot{m}_D (g/min)	T_A (K)	T_B (K)	$T_{C.in}$ (K)	P_{El} (W)	η_{El} (%)
1	27.2	14.8	301.4	742	318.2	1054.1	11.1
2	26.9	15.1	303.5	741.4	318.1	1048.4	10.9
3	26.4	15	298.1	741.4	319	1050.4	11.2
Average	26.8	15.0	301	741.6	318.4	1051	11.1
B (\pm)	0.6	1	0.3	0.1	0.3	1	0.8
S (\pm)	0.05	0.003	0.43	0.57	0.02	0.59	0.11
U _{95%} (\pm)	0.62	1	1.88	1.3	0.3	16.68	0.84

4.4 Parametric Study

In this section, the WhisperGen Stirling engine set points or engine parameters were varied to analyse their effect on engine power and efficiency. The test range for the parametric study is shown in Table 4-2. For each test, a single variable was increased in the presented range, while all the other variables were kept constant as default values shown in the table.

Table 4-2 Test parameters

Description	Variable	Range	Default	Unit
Inlet air temperature	T_A	300 - 320	300	(K)
Air flowrate	\dot{m}_A	16 - 31	27	(kg/hr)
Diesel flowrate	\dot{m}_D	13 - 17	15	(g/min)

Coolant flowrate	\dot{m}_C	3 - 11	10	(l/min)
Coolant inlet temperature	$T_{C.in}$	295 - 320	305	(K)
Coolant outlet temperature	$T_{C.out}$	315 - 345	320	(K)
Water flowrate	\dot{m}_W	12 - 20	15	(l/min)

Figure 4-8 to 4-13, and 4-17 shows the engine parameters plotted against power output and electrical efficiency. The experimental test results were also compared to similar literature experimental results and calculated thermodynamic results.

4.4.1 Inlet Air Temperature (T_A)

A parametric study on air temperature is critical, as preheated air can significantly reduce the diesel consumption for the same power output. This preheating of inlet air tests is carried out by passing part of the ambient air into exhaust heat exchanger and the system configuration for the preheating is shown Figure 2-2, where ambient air recovers heat from the engine exhaust flue gas.

Figure 4-8 shows the trend of power output and electrical efficiency for a range of inlet air temperatures from 300 – 320 K. The experimental power slightly increased from 989 W to as high as 1014 W with the increase in burner temperature by 5 K with preheating. But this change in power was not reflected in efficiency as the input fuel energy was constant at 9.8 kW and the change in power output was negligible: it varies from 10.5 – 10.9%. Comparing with thermodynamic results, the trend is alike with the experiments, due to the fact that there was a minor change in T_H , which is the Stirling cycle variable used for calculation. Overall, the limited operating range of the air inlet temperature resulted in little change in the engine performance.

4.4.2 Air Flowrate (\dot{m}_A)

Air is the oxidant for combustion and flue gas transfers heat from the combustion chamber to the working fluid. The mass flowrate of air can be manually changed by adjusting the power of the air blower from 60 - 100%, which links to a flow rate of 16 to 31 kg/hr. However, varying the air flowrate with the engine software Micromon is not reliable, as the system is programmed to run at particular equivalence ratio. Thus, the fuel

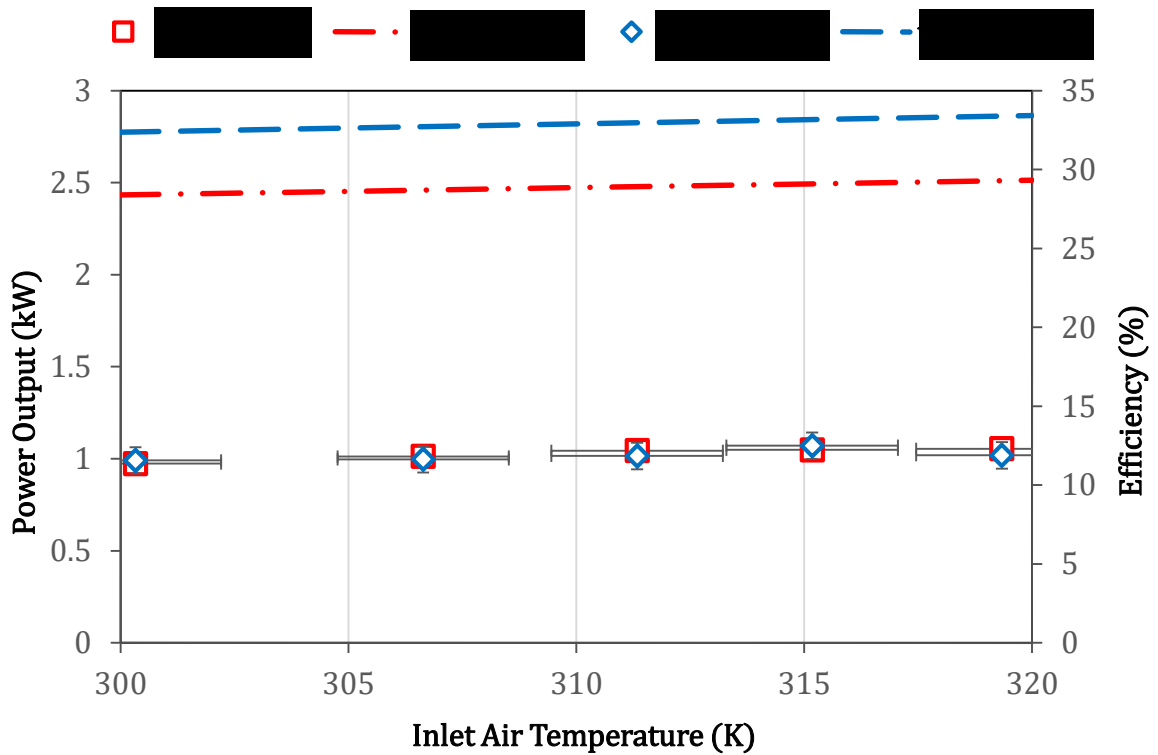


Figure 4-8 Inlet air temperature study

air equivalence ratio must be changed to keep the other engine parameters like the diesel flowrate at its default.

Figure 4-9 shows the trend of power output and efficiency with the increase of air flowrate. The experimental result clearly shows the increase in the mass flowrate of air greatly increased the power output to a maximum power of 1.05 kW at an airflow of 31 kg/hr. When the airflow was set to a lower value, the power output in the steady state period was as low as 700 W. This trend is similar to the literature experimental results by Cacabelos in 2014 [47]. For a higher air flow rate, the efficiency trend is pretty similar with about 4% increase. Comparing with thermodynamic calculation, the trend is almost constant, due to the fact it is accompanied by a mild increasing hot temperature.

For air mass flows less than 20 kg/hr, the system was highly instable; due to improper combustion, the system took an exceeding long time to stabilize or prematurely shutdown; a similar observation was reported [47]. Finally, the performance of the engine increases with air flow, as leaner combustion and higher heat transfer rate result.

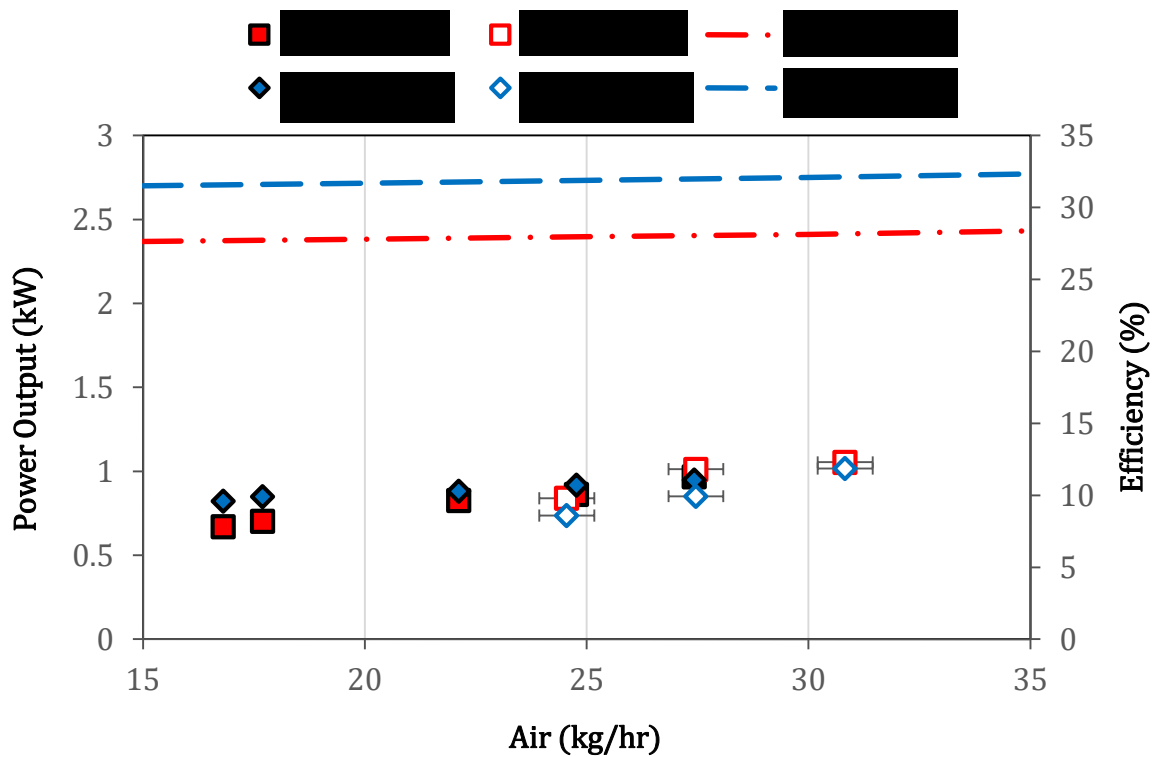


Figure 4-9 Air flowrate study

4.4.3 Diesel Flowrate (\dot{m}_D)

A parametric study on diesel fuel flowrate is important, as engine operation is primarily based on the exhaust temperature set point and this highly dependent on the combustion mixture. Varying the diesel flow using pump frequency in the engine's software is inadequate, as the engine is preprogrammed operating condition. To overcome that, the oxygen sensor set point was varied which altered the fuel to air equivalence ratio in the combustion mixture.

Figure 4-10 demonstrates the diesel mass flow behaviour vs engine performance. As expected, an increase in the fuel flow achieved a higher power output, as this was accompanied with a substantial increase in the burner temperature (15 – 18 K), which correlated to the power efficiency of the engine. This increase in power from 856 W to 1059 W was accompanied with a slight increase in power and efficiency, and almost constant energy efficiency above 14 g/min, due to the increase in fuel energy input. A similar trend was reported by Farra et al. in 2012 [32], but the comprehensive electrical

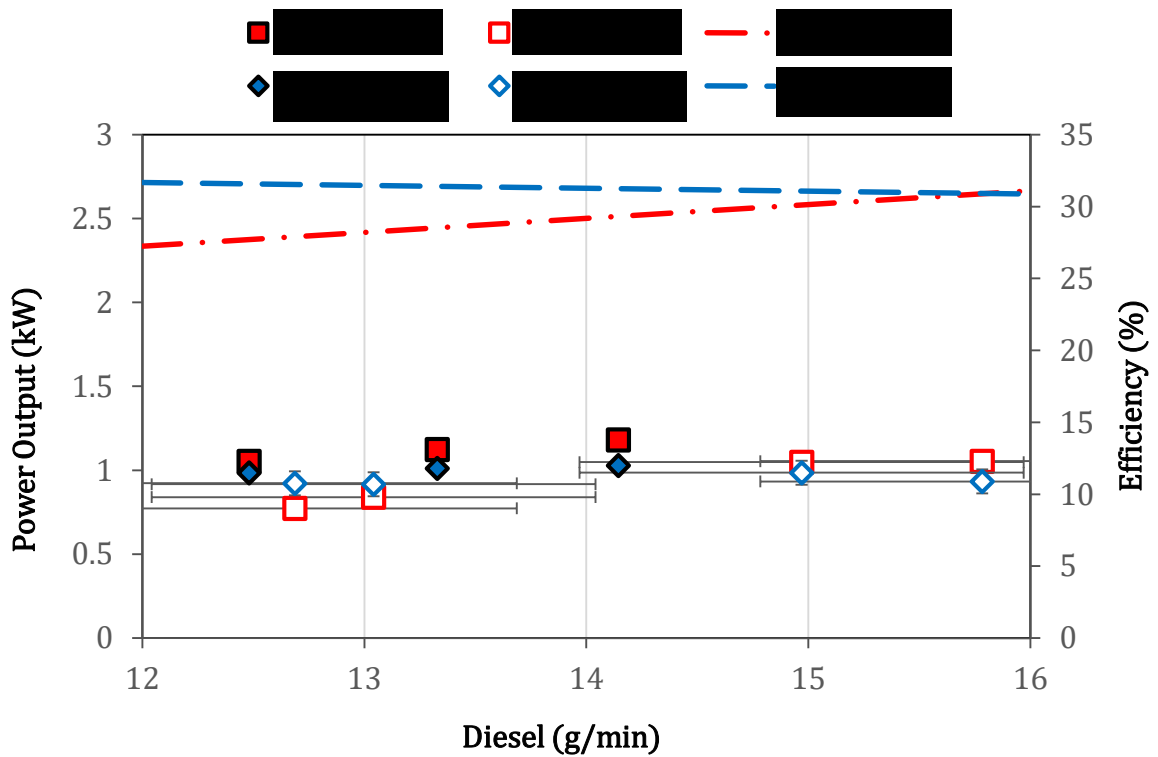


Figure 4-10 Diesel flowrate study

output is about 10 % higher than the present experimental results. This lower engine power was due to damaged hot side heat exchanger ceramic seals. The thermodynamic calculation shows a similar trend with the test results ranging from 2.4 – 2.75 kW power with corresponding efficiency of 32%, nearly three times the experimental results. Repeatedly, the efficiency is almost constant with the increase in power output with diesel input. Overall, the power output increased with higher diesel flow, at almost constant energy efficiency.

4.4.4 Coolant Flowrate (\dot{m}_c)

The coolant flowrate should affect the rate of heat extraction from the compression space of the engine and is necessary for optimum performance. For the parametric study, the coolant was pumped using a constant flowrate pump and the flow was varied using a manual ball valve.

Figure 4-11 shows the constant power output with flowrate. The maximum steady state power of 1 kW and decrease in power with less heat extraction time was also noted

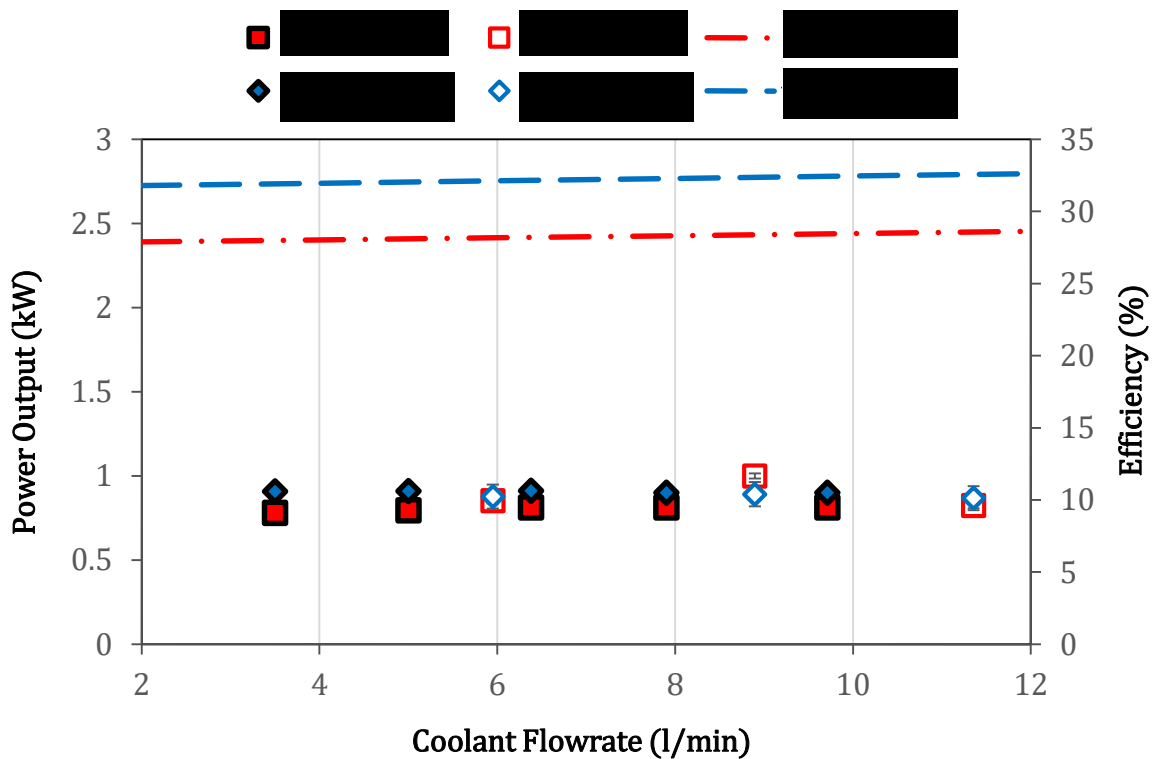


Figure 4-11 Coolant flowrate study

by Lombardi in 2008 [36]. The increase in power output without an increase in energy input, increased the efficiency from 10 – 11%. The thermodynamic calculation inculcates, the coolant flow as the cold side temperature and as this was maintained constant, there was no notable change.

The power output reported in the literature [36] by doing the same experiment is slightly less than the present experimental test, but the power efficiency is the same with a 10.5% average. Overall, the variation of coolant flowrate had very minimum effect on the performance of the Stirling engine and this agrees with the related work and thermodynamics calculation.

4.4.5 Coolant Inlet Temperature ($T_{C.in}$)

The temperature of the coolant is important, as this increases the temperature difference in the Stirling engine. This was varied by increasing the water flow rate across the secondary heat exchanger, as shown in Figure 3-1.

Figure 4-12 shows the effect of coolant inlet temperature on the WhisperGen engine performance. The experimental power clearly decreased with the increase in coolant temperature, i.e. with an increase of 20 K, the power output was reduced by 150 W. This decrease in power, decreased the efficiency by 2%, with a constant energy input. A similar trend was found by Lombardi in 2008 [36], with highest power of about 1 kW and power efficiency of 10.5% at 298 K. The declining tendency is also comparable with the thermodynamic analysis, where the calculated engine performance is less for higher coolant temperatures. Overall, the WhisperGen power and efficiency was greater at low coolant temperature and this coolant temperature have much higher effect on power compared to the coolant flowrate.

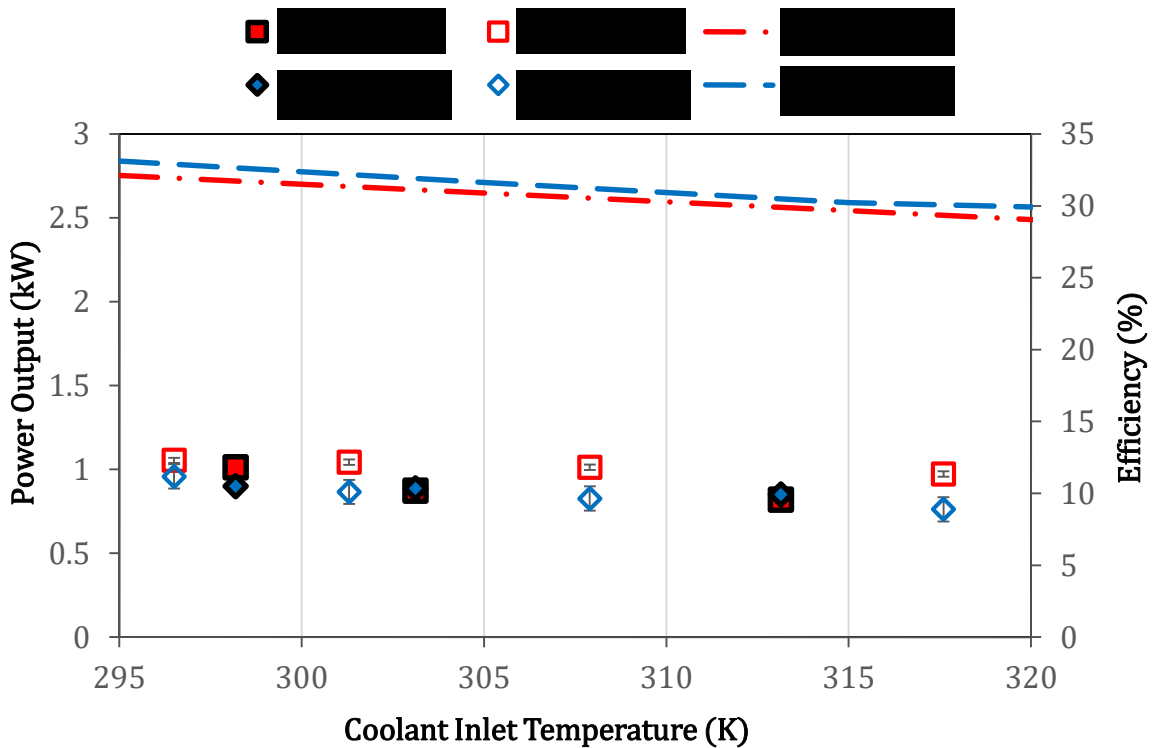


Figure 4-12 Coolant inlet temperature study

4.4.6 Coolant Outlet Temperature ($T_{C.out}$)

The results of the coolant outlet temperature study are shown in Figure 4-13 and is a different parameter from coolant inlet temperature, as it is highly depended on the clamp

element. This parametric study is accomplished by varying the block temperature set point from 315 – 340 K.

The performance of the engine decreased with the coolant temperature from the rated value of 1000 W to as low as 836 W at highest coolant outlet temperature of 342 K. This increase in temperature by varying block temperature set point decreased the power output but gave a constant thermal output. Ulloa, in 2013 [35], recorded a similar power decrease with increase in coolant temperature. The efficiency of the system decreased with the same increase in temperature from 10.1 to 8.6%, and again this change was due to output as the energy input was constant. The thermodynamic trend is alike the previous parametric study, as both variables affect the cold side temperature, but the difference is with respect to higher cold temperature. In summary, lowering the coolant temperature raised performance, due to the fact that lower temperature resulted in better heat extraction.

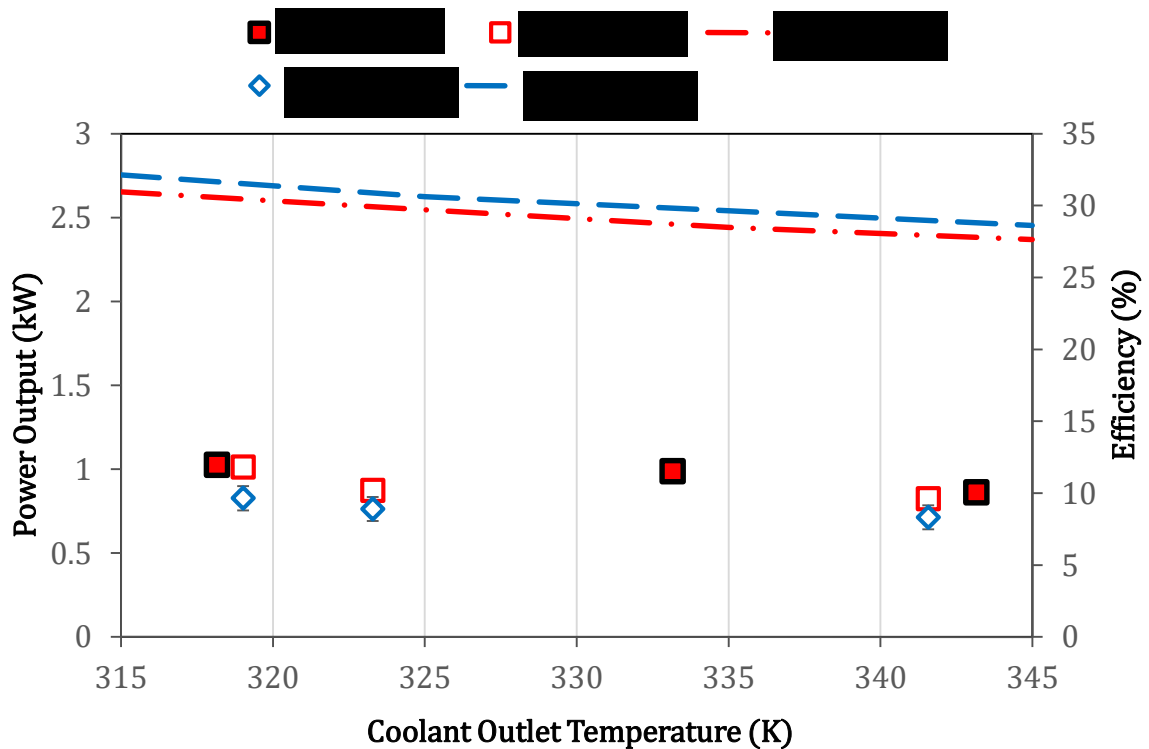


Figure 4-13 Coolant outlet temperature study

4.5 Beale Number Analysis

Figure 4-14 shows the quantitative estimate based on the Beale number obtained for a WhisperGen Stirling engine at various burner temperatures. The power output based on the Beale number is calculated from the Beale formula in Equation 2-38 with engine specifications of 25 Hz, 35 bar, an expansion volume of $3.414 \text{ E-}05 \text{ m}^3$, and Beale numbers from Figure 2-6 for particular burner temperatures. This shows that the Beale number increases with increasing hot temperature and ranges from 0.007 – 0.01. Next, the experimental power output was compared to the power output calculated from the Beale formula and the result follows the same trend.

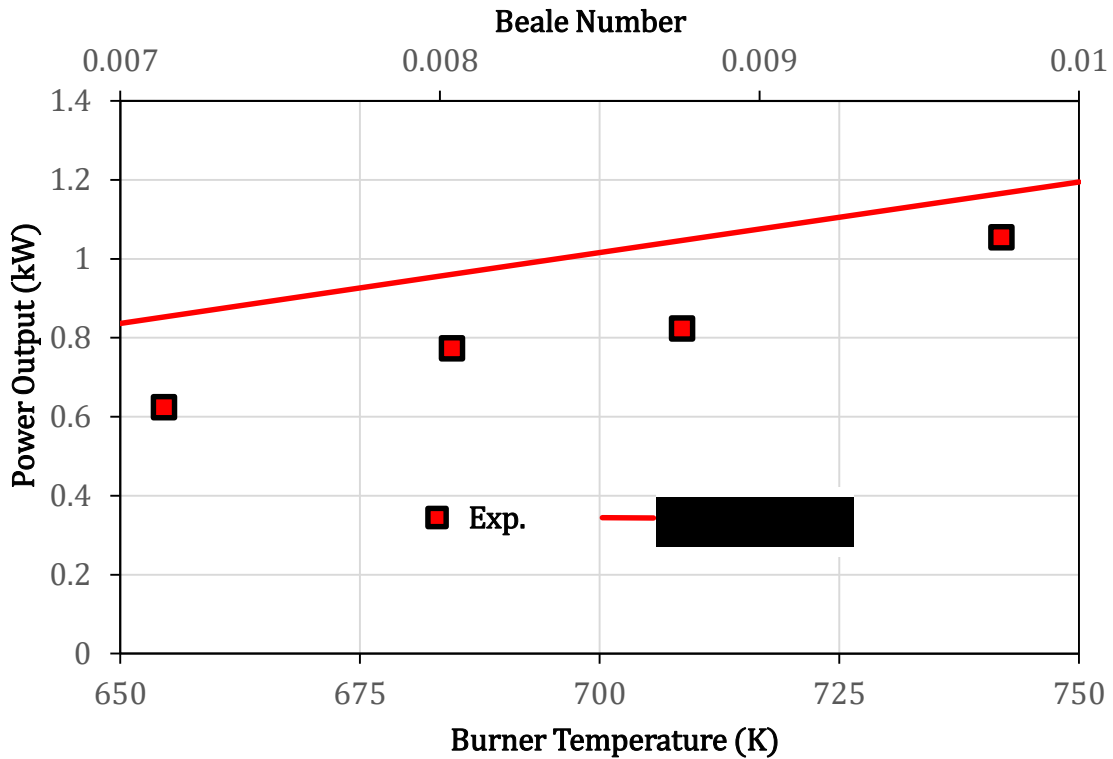


Figure 4-14 Quantitative estimate of Beale number

4.6 Engine Performance with Heat Recovery

This section describes the performance of the WhisperGen Stirling engine from both electrical and thermal output / efficiency point of view, thereby calculating the total energy output and comparing it to the total input energy and losses. The total energy loss

from the system is also compared to the energy loss from engine performance calculations without heat recovery.

Energy input (\dot{Q}_{In}) is the total energy supplied to the system from the combustion of diesel fuel and is calculated from mass flowrates and specific enthalpies of air and diesel. In Figure 4-15, the input energy increases drastically with fuel, and attains steady state at about 10 kW thermal input. The total energy input is converted into two different work outputs. First is the electrical output (P_{EI}) from the alternator by mechanical motion of the heat converter Stirling engine, discussed in an early engine performance section. Next, the remaining heat in the exhaust flue gas is recovered by laboratory cold water in the exhaust heat exchanger and this heat output from the system is called thermal output, \dot{Q}_{Th} (Equation 2-5). This gradually increased with exhaust temperature and took a large amount of time to stabilize, but reached a steady-state around 7.5 -7.75 kW.

The total useful output (\dot{Q}_{To}) of the WhisperGen system is the sum of electrical and thermal outputs and was around 8.5 kW. This total output was only slightly above the

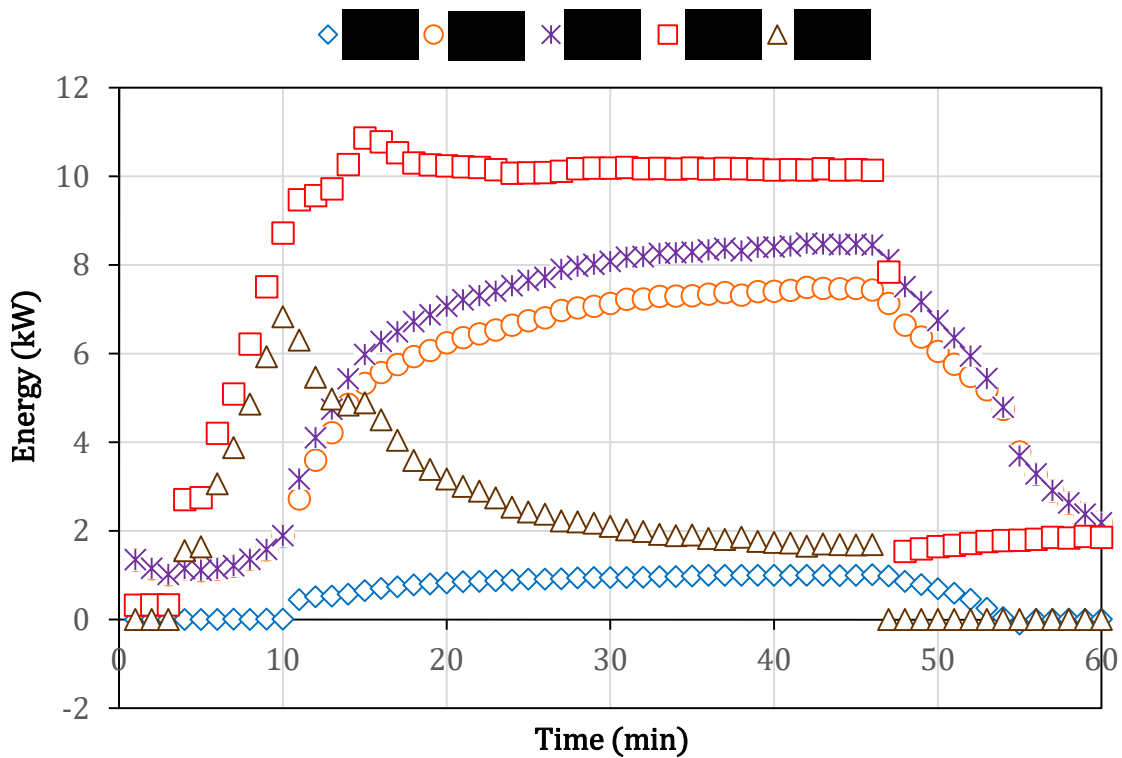


Figure 4-15 Energy balance of WhisperGen with heat recovery

thermal output, as \dot{Q}_{Th} was the major contributor. This total output greatly reduced the energy loss in the system, i.e. from 9 kW when the system was run without heat recovery to around 2 kW with heat recovery (Figure 4-16). Again, the remaining losses were through convection or radiation and heat loss in the exhaust. Initially, a higher portion of heat (about 7 kW) was lost in the exhaust as the heat input was higher and relatively low heat recovery in the exhaust heat exchanger.

Figure 4-17 illustrate the transient nature of the power, thermal, and total efficiencies of the Stirling engine system. A considerable amount of time is needed for system efficiencies to reach their steady state values as calculated from Equations 2-2, 2-8, and 2-9. The system achieved a power efficiency of 11.1%, thermal efficiency of 73.3% and total efficiency of 84.4%.

Theoretically this curve should reach 100%, but the practical energy efficiency was less due to the presence of losses. The low power efficiency of this Stirling engine is primarily due to the choice of the working fluid and its mean cycle pressures. It has been

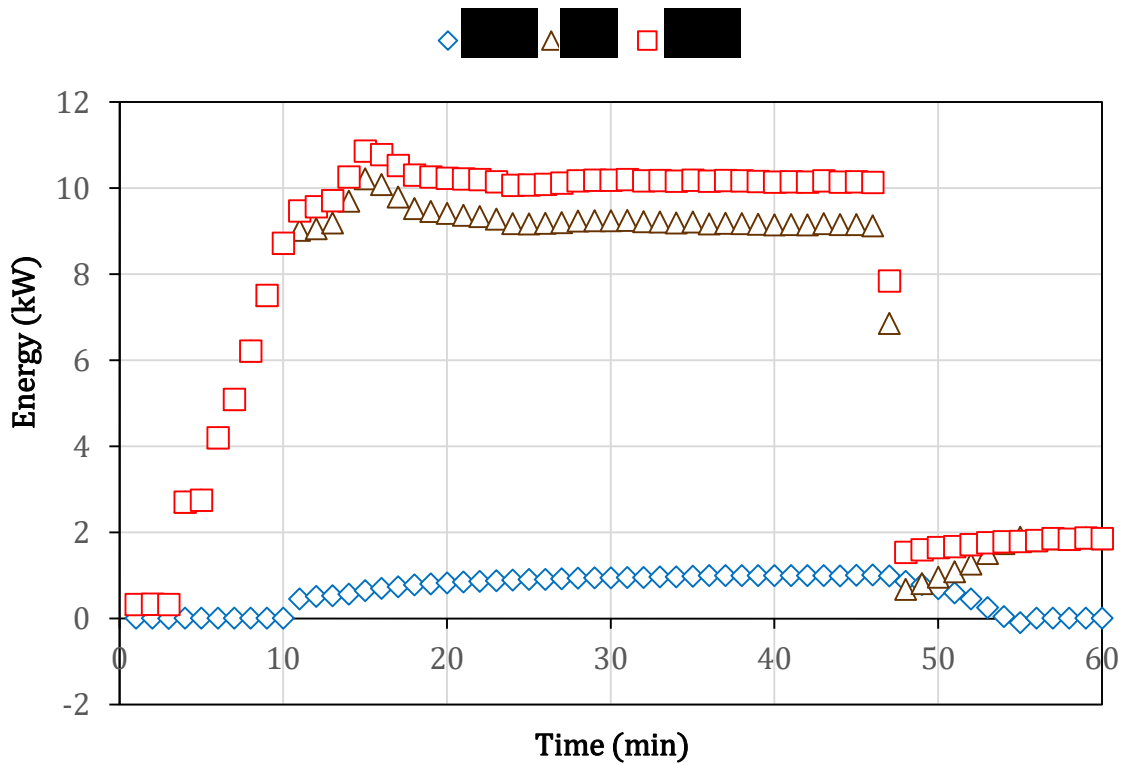


Figure 4-16 Energy balance without heat recovery

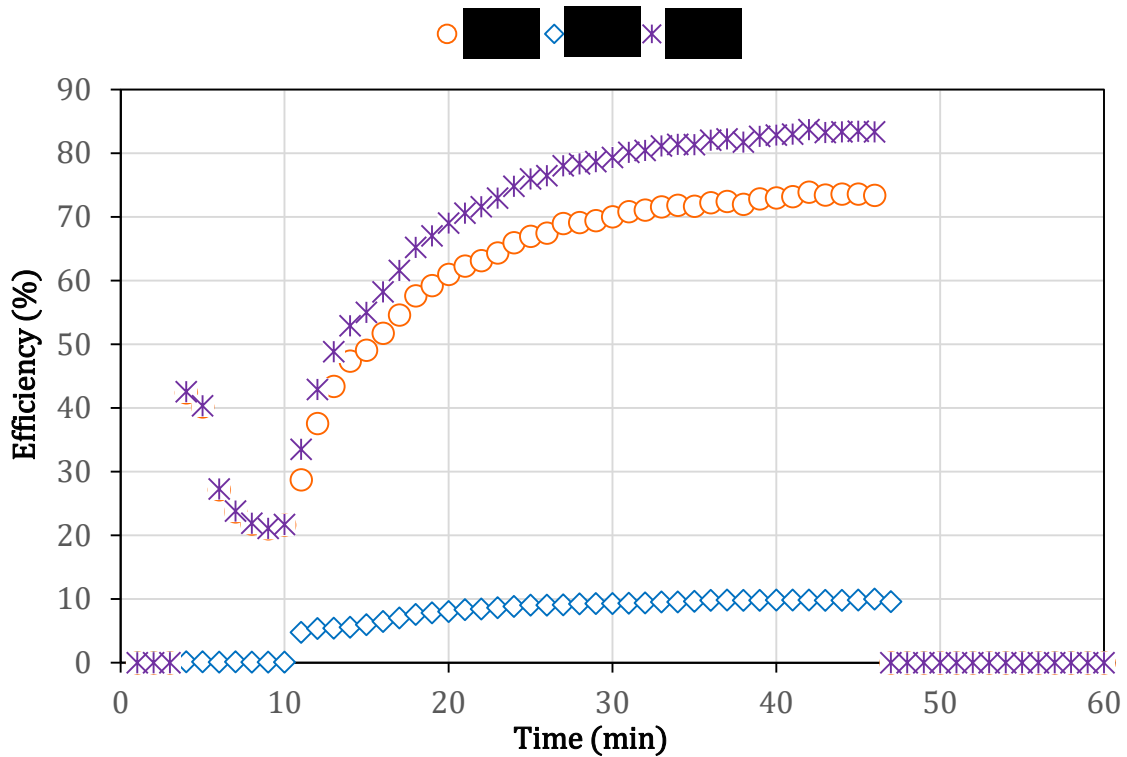


Figure 4-17 LHV efficiency of WhisperGen system

shown previously that nitrogen has poor heat transfer and fluid friction properties, making it an inferior working fluid. Also, mean cycle pressures in the range of 10 – 20 MPa are required to achieve a high power efficiency with N₂, whereas the working fluid in WhisperGen engine is pressurized only at 2.8 MPa [43].

4.6.1 Parametric Study of Water Flowrate (\dot{m}_W)

The water flowrate across the two heat exchangers is important, as it affects the thermal power and efficiency of the WhisperGen. So, this section discusses the final variable in the parametric study indicated in Table 4-2. The effect is shown in Figure 4-18. For the tests, the flow of water was varied with a manual valve, this changed the flow rate from 11 – 19 l/min, and all the other variables were maintained at default value. The results distinctly show the increase in thermal power from 7.75 – 8.05 kW with the increase in flow by 6 l/min and this increased the total output of the system to 9 kW. The main reason behind the change in thermal power with flowrate, was due to the very high flowrate of the exhaust flue gas. Thereby sufficient flow is necessary to recover heat from a flue gas

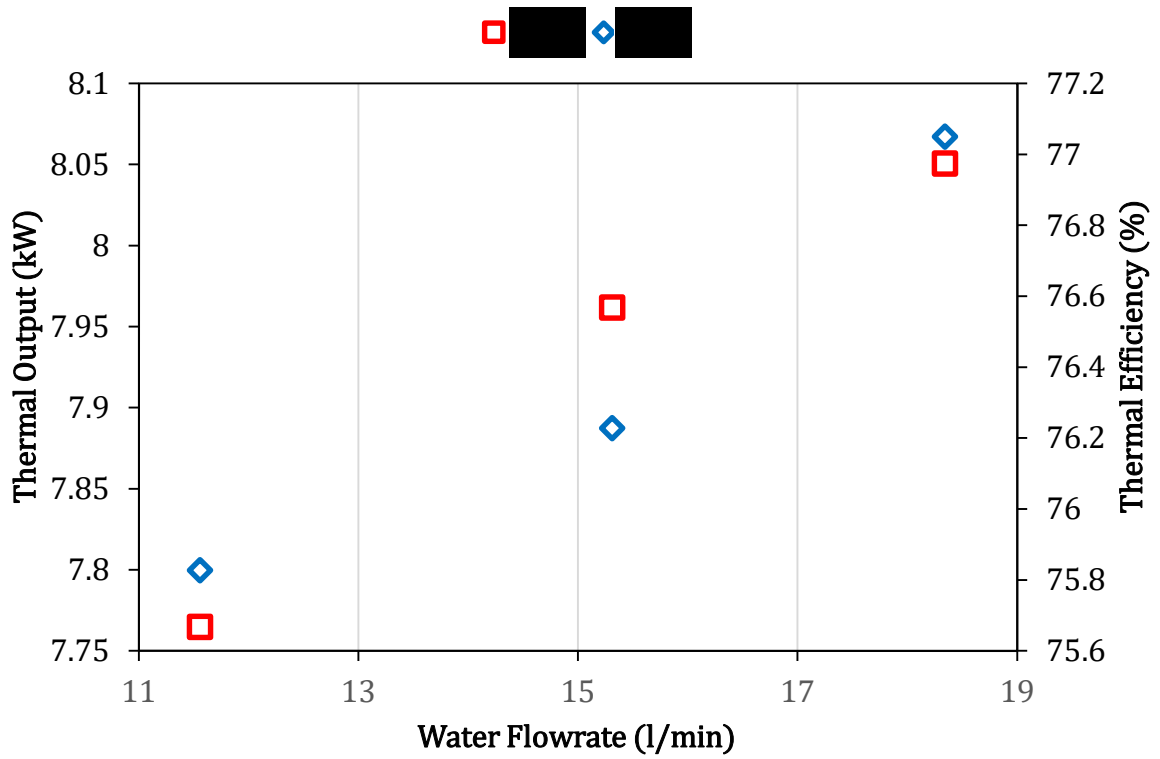


Figure 4-18 Water flowrate behavior

flowing at 270 l/min and this will limit the loss of heat in the exhaust and increase thermal efficiency by 1.3%.

CHAPTER 5

CONCLUSIONS AND RECOMMENDATIONS

5.1 Conclusions

The objective of this thesis was to commission the 12V DC WhisperGen Stirling engine burning diesel with necessary components and instruments to operate the test apparatus and to calculate power and thermal performance.

The experimental data are highly transient and the few system temperatures took a long time for stabilization. For precision of the test results the uncertainty analysis was also performed to verify the accuracy of each measured and derived parameter. The repeatability test shows that the engine performance was 99% reproducible. The experimental setup produces an average power output of 1 kW and power efficiency of 10.5%.

The parametric study on engine parameters: inlet air temperature, air flowrate, diesel flowrate, coolant flowrate, coolant inlet temperature, coolant outlet temperature, and water flowrate has shown interesting effects on engine performance:

- Preheating the inlet air has resulted in no notable effects on the performance of the Stirling engine, in spite of recovering heat from the exhaust, and this is due to the low air temperature range: from 300 to 320 K.
- Air flowrate had a much higher effect than preheating on the engine power output and efficiency, as this was responsible for the heat transfer between the combustion chamber and the Stirling engine's working fluid. The study showed that, the elongated time for attaining steady state for any low flowrate less than 20 kg/hr,

and early shutdown for any flowrate below that, was a result of not enough oxidant for combustion.

- Increasing the diesel flowrate from 13 - 17 g/min resulted in higher power output, as increased fuel flowrate means richer combustion and a higher burner temperature. However, efficiency had a different trend, it increased initially and decreased with a higher diesel energy input.
- The coolant flowrate across the engine block enhanced the compression work, thereby for a higher flow rate of 10 l/min or above, it resulted in a decrease in power output, as there was less time for heat transfer.
- Decreasing coolant temperature had a greater effect on performance than its flowrate. As it increased, the temperature difference resulted in a 2 – 3% increase in power efficiency. Coolant inlet temperature had a much higher influence, due to the fact that the lower temperature in the inlet results in better heat extraction, whereas coolant outlet temperature was highly affected by the clamp element.

The thermodynamic analysis was carried out based on an energy analysis to validate the experimental results of the WhisperGen Stirling engine. The comparison showed about 2.5 to 3 times higher thermodynamic power and efficiency compared to experimental results, and the overall trend was common for all parameters. Further, the power estimate based on the Beale formula followed the same trend as the experimental power for the Beale number range of 0.007 – 0.01.

Finally, the experimental testing was extended to the Stirling engine with heat recovery, where the heat is recovered from the engine coolant and the exhaust flue gas for thermal output. Furthermore, this increases the overall performance of the engine to 85.4% with an average thermal output of 8 kW.

5.2 Recommendations

In this study, the Stirling engine is powered by diesel, which is a high grade fossil fuel, and widely used in IC engines. As Stirling engine features external combustion, a wide range of energy sources can be used as input energy. It is recommended that the

Stirling engine be used with fuels like solid biomass through development of a gasifier, or solar energy.

In order to improve the Stirling engine's power efficiency, a suitable working fluid at much higher pressure is mandatory. Particularly for high power output of a small engines, either hydrogen or helium will be ideal choice and much better alternative to nitrogen.

For higher Stirling engine efficiency, the hot to cold temperature difference has to be higher, but in this WhisperGen MicroCHP, the cold side temperature was highly optimized by the clamp element. So, it is necessary to account for this electrical load from affecting engine performance.

REFERENCES

- [1] Nyboer, J., M. Bennett, M. Wolinetz, N. Melton. "Cogeneration Facilities in Canada 2014." Canadian Industrial Energy End-use Data and Analysis Centre, Simon Fraser University, Burnaby, BC, 2014.
- [2] Walker G. Stirling engines. Oxford: Clarendon Press, 1980.
- [3] Organ, A. J. Stirling Cycle Engines: Inner Workings and Design. John Wiley & Sons, 2013.
- [4] Cengel, Y. A., and M. A. Boles. Thermodynamics: an engineering approach. Edited by Mehmet Kanoğlu. Vol. 5. New York: McGraw-Hill, 2002.
- [5] Finkelstein, T., and A. J. Organ. Air engines: the history, science, and reality of the perfect engine, ASME Press, 2001.
- [6] Martaj, N., L. Grosu, and P. Rochelle. "Exegetical analysis and design optimization of the Stirling engine." International Journal of Exergy 3, no. 1 (2005): 45-67.
- [7] "Engineering ToolBox." Engineering ToolBox. Accessed December 15, 2015. http://www.engineeringtoolbox.com/specific-heat-capacity-gases-d_159.html.
- [8] Martini, W. R. Stirling engine design manual. No. DOE/NASA/3152-78/1; NASA-CR-135382. Washington Univ., Richland (USA). Joint Center for Graduate Study, 1978.
- [9] Kongtragool, B., and S. Wongwises, "A review of solar-powered Stirling engines and low temperature differential Stirling engines." Renewable and Sustainable Energy Reviews 7, no. 2 (2003): 131-154.
- [10] Clucas, D. M. "Development of a Stirling engine battery charger based on a low cost wobble mechanism." PhD dissertation, University of Canterbury, 1993.
- [11] Thombare, D. G., and S. K. Verma. "Technological development in the Stirling cycle engines." Renewable and Sustainable Energy Reviews 12, no. 1 (2008): 1-38.

- [12] Kaushik, S. C., and S. Kumar. "Finite time thermodynamic evaluation of irreversible Ericsson and Stirling heat engines." *Energy Conversion and Management* 42, no. 3 (2001): 295-312.
- [13] Ross, B. A. "Stirling machines and atmospheric emissions." In *Energy Conversion Engineering Conference, 1989. IECEC-89., Proceedings of the 24th Intersociety*, pp. 2331-2336. IEEE, 1989.
- [14] Schmidt, G. "Classical analysis of operation of Stirling engine." A report published in *German engineering union (Original German)* 15 (1871): 1-12.
- [15] Hoegel, B. "Thermodynamics-based design of stirling engines for low-temperature heat sources." PhD dissertation, University of Canterbury, 2014.
- [16] Haywood, D., J. K. Raine, and M. A. Gschwendtner. "Investigation of seal performance in a 4- α double-acting Stirling cycle heat-pump/refrigerator." *Proceedings of the 10th International Stirling Engine Conference and Exhibition*, Osnabrück, 2001.
- [17] Onovwiona, H. I., and V. I. Ugursal. "Residential cogeneration systems: review of the current technology." *Renewable and Sustainable Energy Reviews* 10, no. 5 (2006): 389-431.
- [18] Chung, S. K., and Y. Song. "Design of power conversion system for Stirling engine Micro-CHP integrated into DC power distribution network." In *Telecommunications Energy Conference (INTELEC), 2011 IEEE 33rd International*, pp. 1-8. IEEE, 2011.
- [19] Kongtragool, B., and S. Wongwises. "A four power-piston low-temperature differential Stirling engine using simulated solar energy as a heat source." *Solar Energy* 82, no. 6 (2008): 493-500.
- [20] Cullen, B., and J. McGovern. "Energy system feasibility study of an Otto cycle/Stirling cycle hybrid automotive engine." *Energy* 35, no. 2 (2010): 1017-1023.
- [21] "WP-5012-001-01 DC Marine User's Manual", Whisper Tech Limited, Christchurch, New Zealand, 2005.

- [22] Aguirre, A. A., E. G. Canseco, and J. Scherpen. "Linear dynamics and control of a kinematic wobble-yoke Stirling engine." In Decision and Control (CDC), 2010 49th IEEE Conference, pp. 2747-2752. IEEE, 2010.
- [23] Bell, M., M. C. Swinton, E. Entchev, J. Gusdorf, W. Kalbfleisch, R. G. Marchand, and F. Szadkowski. "Development of micro combined heat and power technology assessment capability at the Canadian Centre for Housing Technology." Ottawa, ON, Canada, Tech. Rep. B-6010, 2003.
- [24] Entchev, E., J. Gusdorf, M. Swinton, M. Bell, F. Szadkowski, W. Kalbfleisch, and R. Marchand. "Micro-generation technology assessment for housing technology." *Energy and Buildings* 36, no. 9 (2004): 925-931.
- [25] Swinton, M. C., E. Entchev, M. Bell, J. Gusdorf, F. Szadkowski, W. Kalbfleisch, and R. G. Marchand. "Adapting and assessing energy conversion technologies for integration in houses." *Proceedings of the Joint NSC-NRC Workshop on Construction Technologies*, pp. 187-194, 2004.
- [26] De Bruyn, A. B. "Integration of combined heat and power generators into small buildings-a transient analysis approach." MAsc thesis, University of Waterloo, 2006.
- [27] De Paepe, M., P. D'Herdt, and D. Mertens. "Micro-CHP systems for residential applications." *Energy Conversion and Management* 47, no. 18 (2006): 3435-3446.
- [28] Kuhn, V., J. Klemeš, and I. Bulatov. "MicroCHP: Overview of selected technologies, products and field test results." *Applied Thermal Engineering* 28, no. 16 (2008): 2039-2048.
- [29] Thomas, B. "Experimental determination of efficiency factors for different Micro-CHP units according to the standard DIN 4709." *Applied Thermal Engineering* 71, no. 2 (2014): 721-728.
- [30] Furness, T., R. Garwood, and T. J. Price. "On development of renewable fuel oil for use in UK domestic space heating applications." *Journal of the Energy Institute* 80, no. 2 (2007): 83-87.
- [31] Aliabadi, A. A., M. J. Thomson, J. S. Wallace, T. Tzanetakis, W. Lamont, and J. D. Carlo. "Efficiency and emissions measurement of a Stirling-engine-based

- residential micro cogeneration system run on diesel and biodiesel." *Energy & Fuels* 23, no. 2 (2009): 1032-1039.
- [32] Farra, N., T. Tzanetakis, and M.J. Thomson. "Experimental determination of the efficiency and emissions of a residential micro cogeneration system based on a Stirling engine and fueled by diesel and ethanol." *Energy & Fuels* 26, no. 2 (2012): 889-900.
- [33] Khan, M. U. "Efficiency and emissions study of a residential micro-cogeneration system based on a modified Stirling engine and fueled by a wood derived fast pyrolysis liquid-ethanol blend." MSc thesis, University of Toronto, 2012.
- [34] Lamont, W. "Experimental Development of a Bio-Oil Burner for a Combined Heat and Power Stirling Engine." MSc thesis, University of Toronto, 2008.
- [35] Ulloa, C., J. L. Míguez, J. Porteiro, P. Eguía, and A. Cacabelos. "Development of a transient model of a stirling-based CHP system." *Energies* 6, no. 7 (2013): 3115-3133.
- [36] Lombardi, K. M. "Investigation of Performance and Simulation Modelling of a Stirling Engine for Residential Cogeneration." MSc thesis, Dalhousie University, 2008.
- [37] Wilson, S., M. Gosden, and I. Povey. "Experiences Gained from the Monitoring of an LV Network Supplying a Micro-CHP Cluster." In *20th International Conference and Exhibition on Electricity Distribution - Part 1, 2009. CIRED 2009*, 1-5, 2009.
- [38] Molderink, A., V. Bakker, M. G. C. Bosman, J. L. Hurink, and G. J. M. Smit. "A three-step methodology to improve domestic energy efficiency." In *Innovative Smart Grid Technologies (ISGT)*, 2010, pp. 1-8. IEEE, 2010.
- [39] Conroy, G., A. Duffy, and L. M. Ayompe. "Validated dynamic energy model for a Stirling engine μ -CHP unit using field trial data from a domestic dwelling." *Energy and Buildings* 62 (2013): 18-26.
- [40] González, P. I., A. C. Celador, E. P. Iribarren, J. T. Zubiaga, and J. M. Sala. "Parametric study of the operational and economic feasibility of Stirling micro-cogeneration devices in Spain." *Applied Thermal Engineering* 71, no. 2 (2014): 821-829.

- [41] Gopal, V. K., R. Duke, and D. Clucas. "Design and development of a test rig to validate the concept of an Active Stirling Engine." In Universities Power Engineering Conference (AUPEC), 2010 20th Australasian, pp. 1-6. IEEE, 2010.
- [42] Pourmovahed, A., T. Opperman, and B. Lemke. "Performance and efficiency of a biogas CHP system utilizing a Stirling engine." In Proceedings of International Conference on Renewable Energies and Power Quality, Las Palmas de Gran Canaria, Spain, vol. 1315. 2011.
- [43] Alanne, K., N. Söderholm, K. Sirén, and I. B. Morrison. "Techno-economic assessment and optimization of Stirling engine micro-cogeneration systems in residential buildings." *Energy Conversion and Management* 51, no. 12 (2010): 2635-2646.
- [44] Peacock, A. D., and M. Newborough. "Impact of micro-CHP systems on domestic sector CO₂ emissions." *Applied Thermal Engineering* 25, no. 17 (2005): 2653-2676.
- [45] Petrescu, S., M. Costea, C. Harman, and T. Florea. "Application of the direct method to irreversible Stirling cycles with finite speed." *International Journal of Energy Research* 26, no. 7 (2002): 589-609.
- [46] Wu, F., L. Chen, F. Sun, C. Wu, and Y. Zhu. "Performance and optimization criteria for forward and reverse quantum Stirling cycles." *Energy Conversion and Management* 39, no. 8 (1998): 733-739.
- [47] Cacabelos, A., P. Eguía, J. L. Míguez, G. Rey, and M. E. Arce. "Development of an improved dynamic model of a Stirling engine and a performance analysis of a cogeneration plant." *Applied Thermal Engineering* 73, no. 1 (2014): 608-621.
- [48] Costa, S. C., M. Tutar, I. Barreno, J. A. Esnaola, H. Barrutia, D. García, M. A. González, and J. I. Prieto. "Experimental and numerical flow investigation of Stirling engine regenerator." *Energy* 72 (2014): 800-812.
- [49] Kongtragool, B., and S. Wongwises, "Thermodynamic analysis of a Stirling engine including dead volumes of hot space, cold space and regenerator." *Renewable Energy* 31, no. 3 (2006): 345-359.

- [50] Duan, C., X. Wang, S. Shu, C. Jing, and H. Chang. "Thermodynamic design of Stirling engine using multi-objective particle swarm optimization algorithm." *Energy Conversion and Management* 84 (2014): 88-96.
- [51] Harrod, J., P. J. Mago, K. Srinivasan, and L. M. Chamra. "First and second law analysis of a Stirling engine with imperfect regeneration and dead volume." *Proceedings of the Institution of Mechanical Engineers, Part C: Journal of Mechanical Engineering Science* 223, no. 11 (2009): 2595-2607.
- [52] Ahmadi, M. H., H. Sayyaadi, A. H. Mohammadi, and M. A. B. Jimenez. "Thermo-economic multi-objective optimization of solar dish-Stirling engine by implementing evolutionary algorithm." *Energy Conversion and Management* 73 (2013): 370-380.
- [53] Tlili, I., Y. Timoumi, and S. B. Nasrallah. "Analysis and design consideration of mean temperature differential Stirling engine for solar application." *Renewable Energy* 33, no. 8 (2008): 1911-1921.
- [54] Feng, J., S. Megerian, and M. Potkonjak. "Model-based calibration for sensor networks." In *Sensors, 2003. Proceedings of IEEE*, vol. 2, pp. 737-742. IEEE, 2003.
- [55] Abernethy, R. B., R. P. Benedict, and R. B. Dowdell. "ASME measurement uncertainty." *Journal of Fluids Engineering* 107, no. 2 (1985): 161-164.

VITA AUCTORIS

NAME: Prashant Kaliram Pradip

PLACE OF BIRTH: Virudhunagar, India

YEAR OF BIRTH: 1991

EDUCATION: Bannari Amman Institute of Technology, B.E. (Mechanical Engineering), Sathyamangalam, India, 2012

University of Windsor, M.Eng. (Mechanical Engineering), Windsor, ON, 2013